ELSEVIER

Arthropod Structure & Development 36 (2007) 77–102

ARTHROPOD STRUCTURE & DEVELOPMENT

www.elsevier.com/locate/asd

Morphology of the prosomal endoskeleton of Scorpiones (Arachnida) and a new hypothesis for the evolution of cuticular cephalic endoskeletons in arthropods

Jeffrey W. Shultz*

Department of Entomology, University of Maryland, College Park, MD 20742-4454, USA

Received 9 April 2006; accepted 3 August 2006

Abstract

Skeletomuscular anatomy of the scorpion prosoma is examined in an attempt to explain the evolution of two endoskeletal features, a muscular diaphragm dividing the prosoma and opisthosoma and cuticular epistomal entapophyses with a uniquely complex arrangement of muscles, tendons and ligaments. Both structures appear to be derived from modifications of the mesodermal intersegmental endoskeleton that is primitive for all major arthropod groups. The scorpion diaphragm is a compound structure comprising axial muscles and pericardial ligaments of segments VI to VIII and extrinsic muscles of leg 4 brought into contact by longitudinal reduction of segment VII and integrated into a continuous subvertical sheet. This finding reconciles a long-standing conflict between one interpretation of opisthosomal segmentation based on scorpion embryology and another derived from comparative skeletomuscular anatomy. A new evolutionary-developmental mechanism is proposed to account for the complex morphology of the epistomal entapophyses. Each entapophysis receives 14 muscles and tendons that in other taxa would attach to the anterior connective endoskeleton in the same relative positions. This observation suggests that the embryological precursor to the connective endoskeleton can initiate and guide ectodermal invagination and thereby serve as a spatial template for the development of cuticular apodemes. This mesoderm-template model of ectodermal invagination is potentially applicable to all arthropods and may explain structural diversity and convergence in cephalic apodemes throughout the group. The model is used to interpret the cephalic endoskeletons of two non-chelicerate arthropods, Archaeognatha (Hexapoda) and Symphyla (Myriapoda), to demonstrate the generality of the model.

Keywords: Tentoria; Apodeme; Endosternite; Comparative anatomy; Development

1. Introduction

Scorpions are traditionally considered morphologically primitive chelicerates, but their prosomal endoskeleton (e.g., Lankester et al., 1885; Snodgrass, 1948; Abd el-Wahab, 1952; Vyas, 1970; Firstman, 1973) differs significantly from the metameric connective endoskeleton typical of other plesiomorphic arthropods (Hessler, 1964; Cisne, 1974, 1981; Boudreaux, 1979; Fanenbruck, 2003; Bitsch and Bitsch, 2002), including many chelicerates (e.g., Xiphosura: Lankester et al., 1885; Shultz, 2001; Araneae: Firstman, 1954, 1973; Palmgren, 1978; Palpigradi: Börner, 1904; Millot, 1942a,b). Specifically, scorpions have a pair of tentorium-like cuticular invaginations (entapophyses) extending rearward from the base of the epistome (= clypeus) and a muscular diaphragm that divides the hemocoel into distinct prosomal and opisthosomal compartments. The cartilage-like endosternite is reduced and its metameric structure is obscured dorsally by enlargement and rearward displacement of cheliceral and pedipalpal muscles and ventrally by anterior displacement of the gonopore and formation of the stomothecal preoral chamber. The goal of the present study is to describe the

* Tel.: +1 301 405 7519; fax: +1 301 314 9290.
E-mail address: jshultz@umd.edu

1467-8039/$ - see front matter © 2006 Elsevier Ltd. All rights reserved.
doi:10.1016/j.asd.2006.08.001

skeletomuscular anatomy of scorpions in order to reconstruct the metameric structure of the prosomal skeletomuscular system, to homologize skeletomuscular elements with those of other arthropods, and to explain the evolutionary origin of the epistomal entapophyses and diaphragm.

The results from this analysis show the diaphragm to be a composite structure assembled primarily from dorsal and posterior oblique endosternal suspensor muscles of the last prosomal segment (postoral segment VI) and the first two opisthosomal segments (postoral segments VII and VIII) as well as extrinsic muscles of leg 4 and pericardial ligaments. These elements were apparently brought into contact through extreme longitudinal reduction of the first opisthosomal segment, an evolutionary transformation that is recapitulated during development and reflected externally as the 'loss' of the pregenital segment (Brauer, 1895). These observations are consistent with the presence of 13 opisthosomal segments in scorpions and resolve a long-standing inconsistency between interpretations based on embryology and those based on comparative skeletomuscular anatomy of adults (e.g., 12 segments by Weygoldt and Paulus, 1979).

Examination of the epistomal entapophyses suggests an evolutionary-developmental mechanism for the formation of entapophyses whereby the embryological precursor to the connective endoskeleton initiates and guides ectodermal invagination. Specifically, the analysis revealed 14 muscles, tendons and ligaments attached to each epistomal entapophysis, including extrinsic appendicular, dorsal and posterior oblique suspensor and pharyngeal dilator muscles, with relative placements essentially identical to those of homologous muscles associated with the mesodermally derived connective endoskeleton in other taxa. It appears that ectoderm invaginated at the epistomal attachment of the connective endoskeleton and that the ectodermal tube was guided through the connective endoskeleton to a point midway through the pedipalpal segment. Muscles, tendons and ligaments that would have attached to the anterior portion of the connective endoskeleton attach instead to the resulting cuticular entapophysis. I term this scenario the mesoderm-template model of ectodermal invagination, and it appears to be capable of explaining the evolution of endoskeletal apodemes throughout Arthropoda.

Traditional scenarios for the origin of endoskeletal elements associated with extrinsic appendicular muscles (i.e., apodemes and transverse endoskeletal ligaments) assume that some of these muscles primitively had sternal attachments (Snodgrass, 1928, 1950, 1958, 1960; Ravoux, 1975) (Fig. 1A). A contralateral pair of such muscles would presumably acquire endoskeletal attachments when either the sternal cuticle invaginated to form an apodeme (Fig. 1B) or when contralateral muscle pairs evolved a tendinous sternal connection that later detached to form a transverse ligament suspended in the hemocoel (Fig. 1C). However, these scenarios are inconsistent with the paucity of unambiguous examples of extrinsic appendicular muscles with sternal attachments and with the currently favored view that a metamerically arranged connective endoskeleton with extrinsic appendicular muscle is a primitive condition for arthropods (Manton, 1964; Cisne, 1974, 1981; Boudreaux, 1979; Fanenbruck, 2003; Shultz, 2001) (Fig. 1D, E). Further, traditional models fail to explain how ectodermal invaginations from one segment could provide attachment for muscles from many segments without invoking multiple *ad hoc* evolutionary events, such as individual muscles shifting attachments from the ventral or dorsal exoskeleton to the 'new' cuticular endoskeleton.

In contrast, the mesoderm-template model proposed here is compatible with current understanding of endoskeletal evolution (reviewed by Bitsch and Bitsch, 2002). Specifically, most arthropod morphologists accept that (1) the arthropod endoskeleton was originally a well-developed, metamerically arranged mesodermal structure with attached extrinsic appendicular muscles, (2) ectodermal invaginations are apomorphic relative to connective endoskeletons, (3) an ectodermal invagination at one segment can pass through several contiguous segments and (4) endoskeletal structures of non-homologous composition (ectoderm vs. mesoderm or cuticle vs. connective tissue) can appear to be homologous in spatial properties (i.e., same morphological placement, similar attachment to homologous muscles). In addition to accommodating accepted hypotheses and observations, the mesoderm-template model predicts that the points and trajectories of ectodermal invagination are determined by the spatial properties of the developmental precursor to the mesodermal connective endoskeleton (e.g., embryological extracellular matrix), such that invaginations are initiated only at points where the connective endoskeleton attaches to the body wall and proceed along trajectories limited by the physical boundaries of the embryonic connective skeleton (Fig. 1E). If this is correct, convergent evolution of endoskeletal apodemes is to be expected and may be exemplified by the anterior tentoria of hexapods and myriapods. The mesoderm-template model is developed further in the Discussion, where the cephalic endoskeletons of Archaeognatha (Hexapoda) and Symphyla (Myriapoda) are interpreted in light of the model.

2. Methods

The study was based on dissection of adult specimens of three scorpion species, *Heterometrus spinifer* (Scorpionidae), *Hadrurus arizonensis* (Iuridae) and *Centruroides vittatus* (Buthidae). Given current understanding of scorpion phylogeny (Stockwell, 1989), similarities among these taxa likely reflect the plesiomorphic condition for extant Scorpiones. Live specimens of *Hadrurus* and *Heterometrus* were obtained from commercial suppliers and maintained in the laboratory for variable durations (weeks to years) and preserved in 95% ethanol within a few hours after death. Preserved specimens of *Centruroides* were obtained from commercial suppliers. Due to the great similarity in prosomal anatomy among these species, the study focused on about 10 specimens of the largest, *H. spinifer*, and results were compared to the others.

All dissections were conducted under a Leica M-10 dissecting microscope at magnifications of 48 to 480× (objective 0.6×, ocular 10×, zoom 8–80×). Drawings were made with the aid of a drawing tube. The study used standard dissection

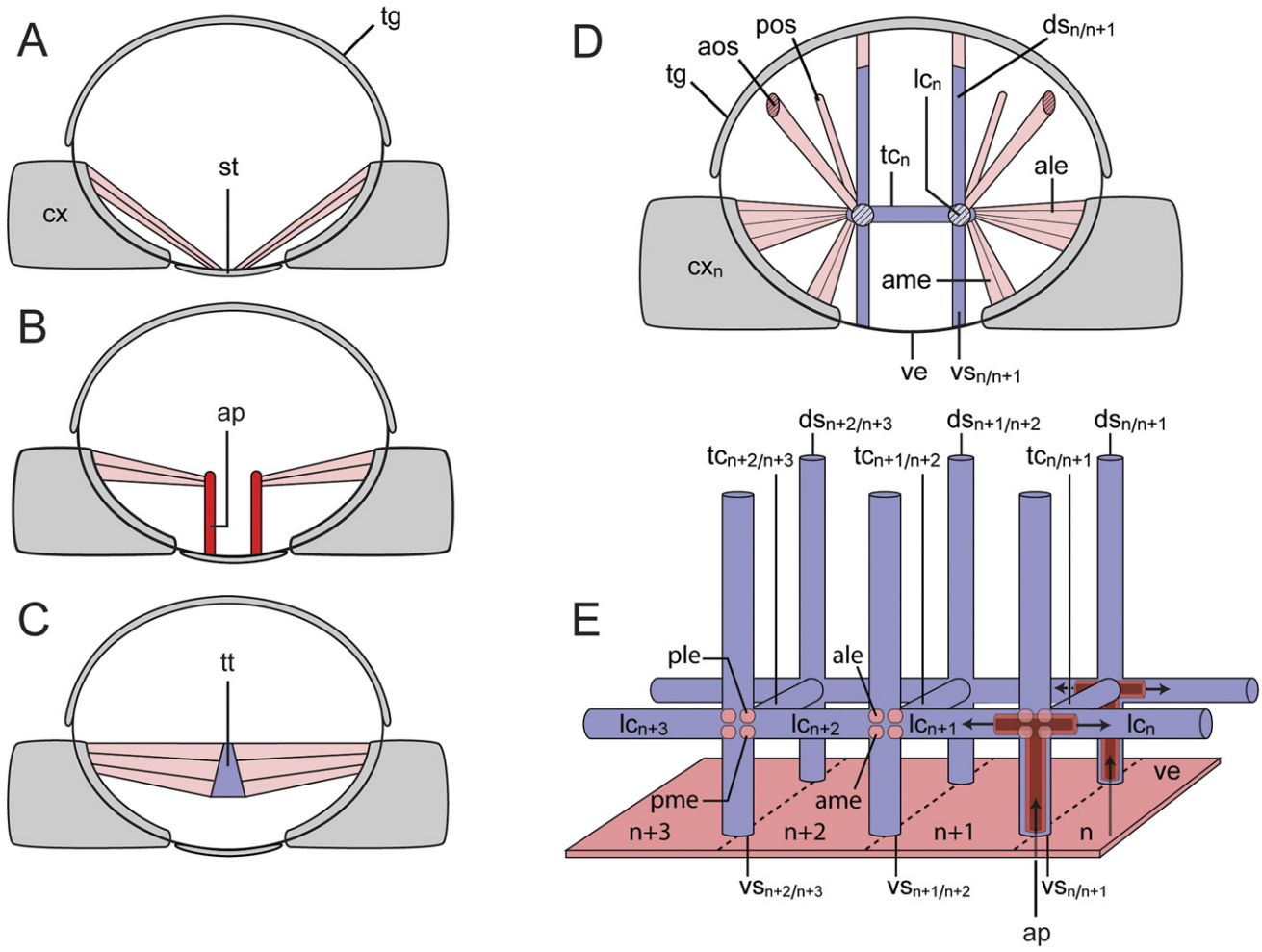

Fig. 1. Snodgrass' model for the evolution of endoskeletal attachments for extrinsic appendicular muscles (A–C) compared to the current concept of the primitive connective endoskeleton of arthropods (D) and the mesoderm-template model of ectodermal invagination (E). (A) Cross section showing hypothetical primitive arthropod with extrinsic coxal muscles attaching to sternum. (B) Traditional explanation for evolution of apodemes and tentoria. Sternal ectoderm invaginates (red) to form endoskeleton and carries extrinsic leg muscles with it. (C) Traditional explanation for evolution of transverse tendons. Extrinsic coxal muscles on opposite sides detach from sternum but retain connection through transverse connective tissue. (D) Anterior perspective of cross section of connective (mesodermal) endoskeleton currently favored by arthropod morphologists (compare with E). Transverse tendons are considered a primitive feature of the endoskeleton and thus do not require explanations such as that proposed by the Snodgrass model. (E) Anterolateral view of primitive mesodermal endoskeleton of arthropods (oblique suspensors *aos* and *pos* removed for clarity), where *n* refers to a postoral body segment. Each coxa has four extrinsic muscles (*ale, ame, ple, pme*) that attach to the endoskeleton. Apodemes (e.g., entapophyses, tentoria) are formed by invaginations of the ventral ectoderm where ventral suspensors attach to the body wall. Ectodermal invagination is guided by the mesodermal template, the embryological precursor to the connective endoskeleton. Abbreviations: *aos*, anterior oblique suspensor; *ap*, sternal apodeme; *cx*, coxa; *ds*, dorsal suspensor; *lc*, longitudinal connective; *n*, number of postoral segment; *pos*, posterior oblique suspensor; *st*, sternite, *tc*, transverse connective; *tg*, tergite; *tt*, transverse tendon; *ve*, ventral ectoderm; *vs*, ventral suspensor. Extrinsic coxal muscles: *ale*, anterior lateral endoskeletal muscle; *ame*, anterior medial endoskeletal muscle; *ple*, posterior lateral endoskeletal muscle; *pme*, posterior medial endoskeletal muscle.

techniques. Cuticular features were cleaned by emersion in warm ~10% KOH solution. Carapacal muscle attachments were mapped by drawing the dorsal surface of an intact specimen and then shaving the cuticle using a sharp scalpel. Most dissections and draws were made from a dorsal perspective, but these were supplemented by prosomata cut sagittally and in cross section.

Muscles of the prosoma (except intrinsic appendicular muscles) and anterior opisthosoma were described (Table 1) and illustrated (Figs. 2–4). Results were compared to those from three relatively thorough studies of scorpion skeletomuscular anatomy (Lankester et al., 1885; Abd el-Wahab, 1952; Vyas, 1970); homologies were established and discrepancies among descriptions were addressed. Scorpion anatomy was compared to that of other chelicerates examined previously by the author—*Limulus polyphemus* (Xiphosura) (Shultz, 2001), *Mastigoproctus giganteus* (Uropygi) (Shultz, 1993), *Phrynus longipes* (Amblypygi) (Shultz, 1999) and *Leiobunum aldrichi* (Opiliones) (Shultz, 2000)—and to those examined in detail by other authors, especially spiders (Firstman, 1954; Palmgren, 1978) and the palpigrade *Eukoenenia mirabilis* (Börner, 1904; Millot, 1942a,b).

Table 1
Prosomal muscles, tendons and ligaments of scorpions

Abbreviation	Description (O = origin. I = insertion)	Homology[a]	Figures
Prosomal doublure, pleural and dorsal longitudinal muscles			
D	O: anteromedial carapace. I: dorsal intercheliceral septum with *PH3*	L 61	Fig. 4C
PL1–PL6	Metameric series. O: lateral carapace. I: *PL1–PL4*, supracoxal pleural membrane; *PL5–PL6*, lateral coxal margin	First record	Fig. 4C
DL1	O: dorsal transverse tendon along anterior margin of tergite 1 deep to *DL2*. I: posterior carapace at subtransverse groove	L 1, V1 *M. dors. long. prosoma*	Fig. 4C
DL2	O: connective membrane between carapace and tergite 1. I: posterior carapace	L 2, V1 *M. dors. obliq. med. prosoma*	Fig. 4C
Labral and epistomal muscles and ligaments (see also C7, C8, ES1, ES2, PH3, PH5, P4, P5)			
EP1	O: medial carapace around optic tubercle. I: posterior median process of epistome	L 62, V1 *M. lat. prosoma I*	Fig. 4B,C
EP2	Forms sling under retracted chelicera. O: supracheliceral carapace. I: ventral intercheliceral septum and adjacent epistome	L 93, V1 *M. lat.-dors. ant.*	Fig. 4B,C
EP3	Forms sling under retracted chelicera. O: anteromedial carapace. I: lateral surface of epistomal entapophysis	L 94, V1 *M. lat.-dors. med.*	Fig. 4B,C
EP4	Sheetlike, muscular and/or tendinous; forms sling under retracted chelicera. O: lateral carapace. I: posterior lateral surface of epistomal entapophysis	L 95, *M. lat.-dors. post.*	Fig. 3B,C
EP5	Attaches to anterior wall of epistome and adjacent surface of labrum on one side, attaches to opposite side	V1 *M. transv. rostri*	Fig. 4B
EP6	O: medial anterior surface of labrum. I: anterior ventral surface of labrum	A 141	–
EP7	O: ventral surface of epistome at base of epistomal entapophysis. I: medial ventral margin of palpal coxa with first subneural connective (*snc1*). May correspond to ventral suspensor of postoral segment II (Fig. 5)	First record	Figs. 2D, 3A
Pharyngeal muscles			
PH1	Fine transverse muscle bands spanning dorsal surface of precerebral pharynx interdigitating with *PH4*	A 130, L 129	–
PH2	Fine subvertical muscle bands spanning lateral surface of precerebral pharynx interdigitating with *PH7*	A 130, L 130,	–
PH3	Long, fine, tendinous. O: dorsal intercheliceral septum near *D.* I: posterior dorsal surface of precerebral pharynx.	A 144, P 'dilator of the pharynx'	–
PH4	O: posterior median process of epistome. I: dorsal surface of precerebral pharynx	A 98, L 98	Fig. 4B
PH5	O: ventral surface of body of epistome. I: dorsal surface of anterior ascending region of precerebral pharynx. Several fibers insert on the oral sclerites with muscle *PH6*	A 142	–
PH6	O: medial margin of palpal coxa or closely associated lateral wall of epistome. I: small 'oral' sclerites embedded in wall of narrow ascending pharynx	First record	–
PH7	O: anterior medial surface of epistomal entapophysis. I: lateral surface of precerebral pharynx. Interdigitates with *PH2*	A 99, L 99, V1 *M. dil. pharyngis lat.*	Fig. 4B
PH8	Circular muscle bands surrounding postcerebral pharynx	A 147	–
PH9	Thin transverse sheet. O: anterior margin of endosternite. Passes anteriorly to anteromedially along the ventral surface of prosomal midgut. I: posterior end of postcerebral pharynx	A 145	Fig. 4B
Extrinsic cheliceral muscles			
C1	O: anteromedial carapace. I: anterior lateral margin of protomerite	L 109, V2 1	Fig. 4A,C
C2	O: anterolateral carapace, posterior to lateral eyes. I: posterior terminus of protomerite surrounded by *C3*	L 120, V2 2	Fig. 4A,C
C3	O: posteromedial carapace. I: posterior terminus of protomerite	L 121, V2 3 + 4	Fig. 4A,C
C4	O: anterior carapace. I: anterior medial margin of protomerite	L 110, V2 5	Fig. 4A,C

C5	O: carapace, posterolateral to median eyes. I: anterior medial margin of protomerite with *C4*	L 110, V2 6	Fig. 3A,C
C6	O: posteromedial carapace. I: dorsal margin of protomerite	L 111, V2 7	Fig. 4A,C
C7	O: posterior medial surface of epistomal entapophysis anteriorly adjacent to *C8*. I: medial margin of protomerite	L 96, V2 10	Fig. 4A
C8	O: posterior medial surface of epistomal entapophysis posteriorly adjacent to *C7*. I: posterior terminus of protomerite	L 97, V2 11	Fig. 4A
C9	O: posteromedial carapace. I: dorsolateral proximal margin of deutomerite	L 106, V2 8	Fig. 4A,C
C10	O: carapace between *C3* and *C5*. I: proximal ventromedial margin of deutomerite	L 107, V2 9	Fig. 4A,C
Extrinsic pedipalpal muscles			
P1	O: lateral carapace Fibers intermingle with *P8* as it passes into coxa. I: mid-dorsal margin of coxa; corresponds to *alc* of ground plan (Fig. 5)	L 112 (?), V1 *M. prom. cox.*?	Fig. 4B,C
P2	O: anterolateral carapace near lateral eyes. I: lateral margin of coxa via tendon. Serial homolog of *L2*; corresponds to *plc* of ground plan (Fig. 5)	L 126, V1 *M. abduct. cox.*	Fig. 4B,C
P3	O: anterolateral carapace near lateral eyes. I: lateral margin of coxa via tendon. Serial homolog of *L3*; corresponds to *pmc* of ground plan (Fig. 5)	L 113, V1 *M. prot. cox.*	Fig. 4B,C
P4	O: posterior ventrolateral surface of epistomal arm. I: ventromedial margin of coxa. Serial homolog of *L4*?; corresponds to *ame* of ground plan (Fig. 5)	First record	Fig. 4B,C
P5	O: dorsolateral surface of epistomal entapophysis. I: anterior dorsomedial margin of coxa. Serial homolog of *L5*?; corresponds to *ale* of ground plan (Fig. 5)	V1 *M. add. cox.*	Fig. 4B,C
P6	O: dorsoanterior surface of anterior endosternal process. I: medial posterior margin of coxa ventral to *P7*. Serial homolog of *L6*; corresponds to pme of ground plan (Fig. 5)	L 72, V1 *M. rem. cox.*	Fig. 4B
P7	O: dorsolateral surface of anterior process of endosternite. I: ventrolateral margin of coxa. Serial homolog of *L7*; corresponds to *ple* of ground plan (Fig. 5)	L 75 + 76, V1 *M. retr. cox.*	Fig. 4B
P8	O: posteromedial carapace. Passes anteriorly with *P9*, fibers intermingle dorsally with *P1* before entering coxa. I: ventral proximal margin of trochanter	L 112: in part, insert. incorrect	Fig. 4B,C
P9	O: posteromedial carapace. Enters coxa ventral to *P8*. I: ventrolateral proximal margin of trochanter. Oblique disk of connective tissue separating anterior and posterior fibers at level of median eye	L 108, V1 *M. dep. tr. post.*	Fig. 4B,C
Extrinsic leg muscles (muscles described in V1 omitted due to numerous errors)			
L1	Serial homolog of *P1*. Corresponds to *alc* in ground plan (Fig. 5)		
L1-1	O: mid-lateral carapace. I: lateral anterior margin of coxa 1	L 114	Fig. 4C,D
L1-2	O: posterior lateral carapace. I: lateral anterior margin of coxa 2	L 115	Fig. 4C,E
L1-3	O: posterior medial carapace. I: anterior lateral margin of coxa 3	L 116	Fig. 4C,F
L1-4	O: posterior medial margin of carapace. Indents anterior surface of diaphragm. I: anterior lateral margin of coxa 4	L 118	Fig. 4C,G
L2	Serial homolog of *P2*. Corresponds to *plc* in ground plan (Fig. 5)		
L2-1	O: mid-lateral carapace. I: lateral margin of coxa 1	L 127	Fig. 4C,D
L2-2	O: mid-lateral carapace. I: posterior lateral margin of coxa 2	L 128	Fig. 4C,E
L2-3	O: posterior lateral margin of carapace. I: posterior lateral margin of coxa 3	L 117	Fig. 4C,F
L2-4	O: posterior lateral carapace. I: lateral margin of coxa 4.	L 119	Fig. 4C,G
L3	Serial homolog of *P3*. Corresponds to *pmc* in ground plan (Fig. 5)		
L3-1	Two parts. *L3a-1*. O: mid-lateral margin of carapace. I: dorsal margin of flange of coxa 1. *L3b-1*. O: pleural membrane dorsal to coxa 1. I: lateral margin of flange of coxa 1	L 122 (= *L3a-1*)	Fig. 4C,D
L3-2	Two parts. *L3a-2*. O: posterior lateral carapace. I: dorsal margin of flange of coxa 2. *L3b-2*. O: pleural membrane dorsal to coxa 2. I: lateral margin of flange of coxa 2	L 123 (= *L3a-2*)	Fig. 4C,E

(*continued on next page*)

Table 1 (*continued*)

Abbreviation	Description (O = origin. I = insertion)	Homology[a]	Figures
L3-3	Small. O: posterior lateral margin of carapace. I: lateral posterior margin of coxa 3	First record	Fig. 4C,F
L3-4	Thin, subtransverse, anteriorly convex sheet; component of diaphragm. O: lateral part of transverse bar of connective tissue of anterior margin of tergite 1. Passes ventrally to ventromedially. I: lateral (distal) posterior margin of coxa 4	First record	Fig. 3C,G
L4	Serial homolog of *P4*. Corresponds to *ame* in ground plan (Fig. 5)		
L4-1	O: anterior terminus of anterior endosternal process. Fans anteriorly. I: medial anterior margin of coxa 1. Associated with $ES10_{III}$	First record	Fig. 4D
L4-2	O: anteroventral projection of anterior endosternal process. I: anterior process of coxa 2. Associated with $ES10_{IV}$	First record	Fig. 4E
L4-3	O: ventral surface of anterior process of endosternite laterally adjacent to $ES10_{V}$. I: anterior end of coxa 3	First record	Fig. 4F
L4-4	May represent anterior part of large muscle with *L6-4*	First record	Fig. 4G
L5	Serial homolog of *P5*. Corresponds to *ale* in ground plan (Fig. 5)		
L5-1	O: lateral margin of terminus of anterior endosternal process of endosternite. I: lateral anterior margin of coxa 1	First record	Fig. 4D
L5-2	O: ventral surface of anterior endosternal process where it comes into contact with the anterior margin of coxa 2. I: anterior medial margin of coxa 2	First record	Fig. 4E
L5-3	O: distal end of lateral process of endosternite. I: anterior margin of coxa 3	L 79	Fig. 4F
L5-4	O: distal end of posterior process of endosternite. I: lateral anterior margin of coxa 4	L 81	Fig. 4G
L6	Serial homolog of *P6*. Corresponds to *pme* in ground plan (Fig. 5)		
L6-1	Two components. *L6a-1*. O: lateral depression of anterior endosternal process. I: dorsal posterior surface of flange of coxa 1. *L6b-1*. O: anterior lateral margin of anterior process of endosternite. Fibers radiate in fanlike sheet. I: entire medial margin of flange of coxa 1	L74	Fig. 4D
L6-2	Two components. *L6a-2*. Small sheet. O: lateral margin of anterior process of endosternite. I: medial margin of coxa 2 at angle formed by base of flange. *L6b-2*. Larger sheet, tendinous. O: lateral margin of anterior process of endosternite (sometimes at a distinct posteroventral projection) immediately posterior to *L6a-2*. I: ventral margin of flange of coxa 2	First record	Fig. 4E
L6-3	O: ventral surface of lateral process of endosternite. I: posterior margin of coxa 3 anteriorly adjacent to *L7-3*	First record	Fig. 4F
L6-4	O: lateral surface of sternal carina. I: adjacent posterior margin of coxa 4. Anterior part may represent *L6-4*	First record	Fig. 4G
L7	Serial homolog of *P7*. Corresponds to *ple* in ground plan (Fig. 5)		
L7-1	Sheetlike. O: marginal projection of anterior endosternal process that adheres to anterior margin of coxa 2. I: posterior surface of flange of coxa 1	First record	Fig. 4D,E
L7-2	O: anterior and dorsal surfaces of lateral process of endosternite and adjacent portions of anterior lateral depression of endosternite. I: medial margin of flange of coxa 2	L 78	Fig. 4E
L7-3	O: posterior lateral depression of endosternite posterior to *L8-3* and anterior to posterior process of endosternite. I: posterior margin of coxa 3	First record	Fig. 4F
L7-4	O: ventral surface of posterior process of endosternite. I: posterior margin of coxa 4. Forms most of diaphragm ventral to endosternite	L 86a	Fig. 4G
L8	No similar muscle in pedipalp		
L8-1	Thin, straplike. O: anterior end of anterior process of endosternite. I: anterior margin of trochanter 1	L 73	Fig. 4D
L8-2	Large. O: anterior lateral depression of endosternite anterior to *L7-2*; passes anterolaterally; inserts on anteroventral margin of trochanter of leg 2	L 77	Fig. 4E

L8-3	Large. posterior lateral depression of endosternite posterior to lateral process of endosternite and anterior to *L7-3*. I: anterior margin of trochanter 3	L 80	Fig. 4F
L8-4	Long, thin, straplike. O: terminus of posterior process of endosternite. I: anterior margin of trochanter 4	L 82	Fig. 4G
Endoskeletal muscles and ligaments (see also *P6*, *P7*, *L4–L7*)			
ES1	Ligament. O: anterior medial surface of endosternal horn near anterior end. I: ventral process of epistomal arm. May correspond to endosternal tissue of posterior half of segment II (Fig. 5)	L described but not named	Figs. 2C, 3A, 4B
ES2	Sheetlike. O: connective tissue flap along anterolateral margin of body of endosternite. I: posterior terminus of epistomal entapophysis	First record	Fig. 4B
ES3	Long, thin. O: dorsal surface of anterior process of endosternite just posterior to anterior complex. Passes dorsoposterolaterally between flanges of coxae 1 and 2. I: posterolateral surface of carapace medially adjacent to *L3a-2*	Pocock (1902: fig 21)	Figs. 2C, 3A, 4C
ES4	O: terminus of anterior dorsal process of endosternite with *ES5*. I: posterior median surface of carapace. May correspond to dorsal suspensor of postoral segment VI. Absent in *Hadrurus* (Iuridae) (present study) and *Bothriurus bonariensis* (Bothriuridae) (Pocock, 1902); present in buthids, vaejovids, euscorpiids and scorpionids (Lankester et al., 1885; Pocock, 1902; Abd el-Wahab, 1952; Vyas, 1970)	L 63, V1 *M. lat. prosoma II*, Pocock (1902: *tg4*)	Figs. 3C, 5A,B
ES5	O: posterior surface of anterior dorsal process of endosternite with *E4*. Passes dorsoposteriorly on anterior surface of diaphragm laterally adjacent to pericardium. I: medial transverse bar of connective tissue of anterior margin of first tergite. May correspond to posterior oblique suspensor of postoral segment VI	L 64 (error), V1 *M. lat. prosoma III* (error), Pocock (1902: *tg5*)	Fig. 5A
ES6	Broad, thin, anteriorly convex sheet. O: between anterior and posterior dorsal processes of endosternite with *ES7*. Passes dorsally to dorsolaterally posterior to *ES8*. I: transverse bar of connective tissue of anterior margin of first tergite. May correspond to the dorsal suspensor of postoral segment VII	L 'diaphragm' (in part)	
ES7	Broad, thin, anteriorly convex sheet. O: between anterior and posterior dorsal processes of endosternite with *ES6*. Passes dorsolaterally anterior to *L3-4*, where it becomes a membranous tendon. I: transverse bar of connective tissue of anterior margin of first tergite. May correspond to the posterior oblique suspensor of postoral segment VII	L 'diaphragm' (in part)	Fig. 5A,B
ES8	O: posterior dorsal process of endosternite with *ES9*. Passes dorsomedially, penetrating diaphragm dorsally. I: anteromedial surface of first tergite at sigilla like those of remaining tergites. May correspond to dorsal suspensor of postoral segment VIII	L 65, V1 *M. lat. meso. I*	Fig. 5A,B
ES9	O: posterior dorsal process of endosternite with *ES8*. Passes posterolaterally, penetrates diaphragm between *ES6* and *ES7*, adheres to posterior surface of *L3-4*. I: anterolateral margin of postoral segment IX. May correspond to posterior oblique suspensor of postoral segment VIII	L 83	Fig. 5A,B
ES10	May correspond to ventral suspensor of ground plan (Fig. 5: *vs*). See *EP7*		
$ES10_{III}$	O: ventral terminus of anterior endosternal process ventral to *L4-1*. I: anterior process of coxal 1 with *snc2*. May correspond to ventral suspensor of postoral segment III	First record	Fig. 3A
$ES10_{IV}$	O: medial surface of anterior endosternal process with *L4-2*. I: anterior coxal process of leg 2 with *snc3*. May correspond to ventral suspensor of postoral segment IV	First record	Fig. 3A
$ES10_{V}$	O: ventral surface of anterior endosternal process with *L4-3*. I: anterior margin of coxa of leg 3 with *snc4*. May correspond to ventral suspensor of postoral segment V	L 84, V1 *M. compr. vent.-postoral ent.*, Pocock (1902: *V.P.*)	Fig. 3A

(*continued on next page*)

Table 1 (*continued*)

Abbreviation	Description (O = origin. I = insertion)	Homology[a]	Figures
ES11	O: posterior surface of endosternite lateral to neural canal. I: anterior surface of pectinal chondrite	L 25, V1 *M. vent. long. lat. meso. I*	Fig. 5B
ES12	O: medial surface of posterior process of sternal carina. I: anterior surface of pectinal chondrite	L 86	Fig. 5B
ES13	Small. O: posterior ventral margin of subneural bridge of endosternite. I: near middle of genital operculum	L 85, V1 *M. compr. vent. operc.*	Fig. 5B
ES14	O: lateral posterior surface of endosternite. I: pectinal chondrite	First record	Fig. 5B

[a] Key to homology: A: Abd el-Wahab (1952), first instar *Leiurus quinquestriatus* (Buthidae); L: Lankester et al. (1885), adult *Heterometrus cyaneus* (Scorpionidae), *Euscorpius italicus* (Euscorpiidae); P: Petrunkevitch (1922), embryos *Centruroides insulanus, C. vittatus* (Buthidae); V1: Vyas (1970), adult *Heterometrus fulvipes* (Scorpionidae); V2: Vyas (1974), chelicerae only, adult *H. fulvipes*.

3. Results

3.1. Appendages

3.1.1. Pedal coxae and extrinsic muscles

The generalized pedal coxa of euchelicerates is depicted in Fig. 5C. The coxa articulates with the trochanter distally through anterior and posterior condyles, and the joint is operated by antagonistic muscles. The anterior condyle is associated with the *costa coxalis*, a longitudinal invagination of cuticle (phragma) indicated externally by a sulcus on the anterior wall of the coxa (Figs. 2G,H, 5C: *cc*). The coxae are attached to the body by flexible cuticle and extrinsic muscles. Comparative anatomy of arachnids and outgroup comparison with *Limulus* (Xiphosura) also indicate that each pedal coxa of the arachnid groundplan has nine extrinsic muscles, five arising from the carapace (Fig. 5C: *amc, alc, pmc, plc, lc*) and four from the endosternite (Fig. 5C: *ame, ale, pme, ple*) (Shultz, 1991).

The skeletal anatomy and muscular apodemes of the scorpion leg have been detailed by Couzijn (1976), and intrinsic musculature and relevant literature has been surveyed by Shultz (1989). The pedal coxae of scorpions differ from the hypothetical primitive configuration in several respects. Pedal coxae 1 and 2 each have a large coxapophysis (Fig. 2G,H: *cxp*) that projects anteriorly and forms part of the preoral chamber (Fig. 2A: *pc*), or stomotheca. The posterior internal margin of coxae 1 and 2 extends dorsally and medially into the prosomal hemocoel in the form of broad, thin-walled flanges (Fig. 2G,H: *cxf*) that provide a large surface for attachment of muscles operating the trochanter. In addition, coxae 1 and 2 appear to have rotated almost 90 degrees around their long axes, transforming the primitive anterior surface into a near-dorsal surface; the *costa coxalis* is located dorsally. Due in part to these rotations, the coxae of the pedipalps and first two pairs of legs tend to overlap, forming a near-vertical stack internally (Fig. 2A). Pedal coxae 3 and 4 also appear to have undergone distortion, but this seems to be associated with the anterior displacement of the genital segment into the coxosternal region of the prosoma. Specifically, each coxa has rotated around a vertical axis so as that the primitive medial (proximal) end points more anteriorly and the lateral (distal) end points more posteriorly (Fig. 2A,I). In addition, coxa 4 has undergone substantial transverse compression and its opening to the prosomal hemocoel is greatly narrowed. Scorpions also differ from most other chelicerates in that the posterior margin of coxa 3 and anterior margin of coxa 4 are immovably fused by sclerotization of the intercoxal membrane.

Despite their different shapes and orientations (Fig. 2G–I), the pedal coxae have similar arrangements of seven extrinsic muscles (Fig. 4D–G). Three muscles attach to the carapace (Fig. 4C–G: *L1, L2*) and/or adjacent pleural membrane (Fig. 4C–G: *L3*), an apparent reduction from the primitive five (Fig. 5C). Four muscles attach to the endoskeleton (Fig. 4D–G: *L4–L7*), the primitive number for arachnids (Fig. 5C). The only exception occurs in coxa 4, where one large muscle arises from the lateral surface of the sternal

carina instead of the endosternite and inserts along the proximal medial (posterior) margin of the coxa (Fig. 4G). This muscle may represent *L4*, *L6* or both. It should be noted that muscles *L3* and *L7* of leg 4 contribute significantly to the lateral and ventrolateral surfaces of the diaphragm, respectively (Figs. 4G, 5A,B: *L3-4, L7-4*). The newly discovered ventral endosternal suspensor muscles (Fig. 3: *ES10* or *vs*) described below also attach to the coxae in association with muscle *L4*. An additional extrinsic muscle arises from the endosternite and inserts on the anterior proximal margin of each pedal trochanter (Fig. 4D–G: *L8*).

3.1.2. Pedipalpal coxae and extrinsic muscles

Intrinsic pedipalpal muscles have been examined most thoroughly by Vyas (1970), although several authors have described the muscles operating the chela (e.g., Barrows, 1925; Snodgrass, 1948; Dubale and Vyas, 1968). Extrinsic muscles have been examined by Lankester et al. (1885), Vyas (1970) and the present study. These descriptions are in general agreement, though several inconsistencies are noted in Table 1. Like pedal coxae 1 and 2, the pedipalpal coxa has undergone a rotation about its long axis that transforms the morphological anterior face into the dorsal face (Fig. 2F) (Kästner, 1931). The coxae lie on the dorsal surface of pedal coxa 1, and the medial surfaces of the pedipalpal coxae form the walls of the preoral chamber (Fig. 2A: *pc*). They also resemble the pedal coxae in having seven extrinsic muscles (Fig. 4B). Three muscles take their origin from the carapace (Figs. 4B,C, 5D: *P1–P3*), two from the epistomal entapophyses (*P4, P5*) and two from the endosternite (*P6, P7*). This suggests that *P4* and *P5* are serial homologs of pedal muscles *L4* and *L5* but that their attachment occurs on the epistomal entapophyses rather than the endosternite. Two large extrinsic muscles arise from the posterior part of the carapace, pass into the pedipalpal coxa and attach to the proximal margin of the pedipalpal trochanter (Fig. 4B,C: *P8, P9*), along with additional fibers arising from the walls of the coxa. Previous workers (Lankester et al., 1885; Vyas, 1970) mistakenly described *P8* as inserting on the dorsal margin of the coxa, an error caused by the extensive intermingling of the fibers of *P8* and those of the overlying *P1*, which does attach to the coxa.

3.1.3. Chelicerae and extrinsic muscles

The chelicerae of scorpions are positioned dorsal to the pedipalpal coxae on either side of the labrum (Fig. 2A: *ch*) suspended by extrinsic muscles (Fig. 4A) and a flexible sleeve of conjunctival cuticle; there are no distinct pivot points or condyles to constrain cheliceral movement with respect to the body. Each chelicera has three articles (protomerite, deutomerite, tritomerite) with the deuto- and tritomerite forming the chela (Fig. 2E). Intrinsic cheliceral muscles have been examined in greatest detail by Vyas (1970, 1974) and extrinsic muscles were examined by Lankester et al. (1885), Vyas (1970, 1974) and the present study (Fig. 4A); there are no significant conflicts among these descriptions. The scorpion chelicera is unusual in having two muscles that originate on the carapace and insert on the proximal margin of the deutomerite (Fig. 4A: *C9, C10*), although harvestmen (Opiliones) have one such muscle (Shultz, 2000; Shultz and Pinto da Rocha, in press). All other deutomerite muscles are intrinsic to the chelicera. Scorpions may be unique in having cheliceral muscles arising from the epistome and attaching to the protomerite (Figs. 4A, 5D: *C7, C8*), although some chelicerates have extrinsic cheliceral muscles that arise from the endosternite (e.g., Xiphosura, Araneae, Amblypygi, Thelyphonida) (Firstman, 1954; Palmgren, 1978; Shultz, 1993, 1999, 2001).

3.2. Labrum–epistome complex

The labrum–epistome of euchelicerates is a roughly cylindrical, median cuticular structure that projects anteriorly to anteroventrally above the mouth (Snodgrass, 1948). It is closed distally by a lobe of soft cuticle, the labrum, and opens to the prosomal hemocoel proximally. The proximal portion, the epistome, is sclerotized dorsally and laterally to form an arch-like sclerite; the ventral surface is flexible and continuous proximally with the dorsal surface of the anterior part of the digestive tract, the precerebral pharynx. The epistome attaches to the body in a variety of ways but often has a strong connection to some portion of the pedipalpal coxae. The labrum and epistome often have three intrinsic muscles, a transverse muscle that spans the epistome and two dorsoventral muscles, one anterior to the transverse muscle that attaches to the ventral surface of the labrum and one posterior to the transverse muscle. Extrinsic muscles are generally limited to dorsoventral muscles of the posterior part of the epistome that dilate the pharynx, although the distinction between the posterior dorsoventral muscle and pharyngeal dilator muscle is not always clear. In some chelicerates, the endosternite terminates anteriorly on or immediately adjacent to the base of the epistome as either a muscle or tendon (Shultz, 2000, 2001; Palmgren, 1978).

The scorpion labrum and epistome retain the basic characteristics described above but have undergone further elaboration. The labrum (Figs. 2A,F, 4B: *lr*) is comparatively very large and fills most of the preoral chamber (Fig. 2A: *pc*) but is otherwise rather simple. In contrast, the epistome (Figs. 2A,D,F, 4A,B: *epstm*) is very complex and has three main parts (Fig. 2D), a central body (*b*), a pair of lateral walls (*lw*) and a pair of entapophyses (*ee*). The body of the epistome is heavily sclerotized and has short anterior and posterior median processes (Fig. 2D: *amp, pmp*), the dorsal surfaces of which have been brought into contact by a deep transverse folding of the dorsal surface. The posterior process gives the appearance of having been folded so far anteriorly that its original ventral surface faces dorsally. The epistomal body has a tight but moveable articulation with the dorsomedial margins of the pedipalpal coxae. The lateral walls of the epistome (Fig. 2D: *lw*) are roughly oval plates of cuticle that attach to the ventrolateral surface of the epistomal body via narrow, flexible articulations. The lateral (external) surface of each plate is broadly and firmly fused to the medial surface of the pedipalpal coxae. The epistomal entapophyses (Fig. 2D: *ee*) are a pair of stiff cuticular processes that project

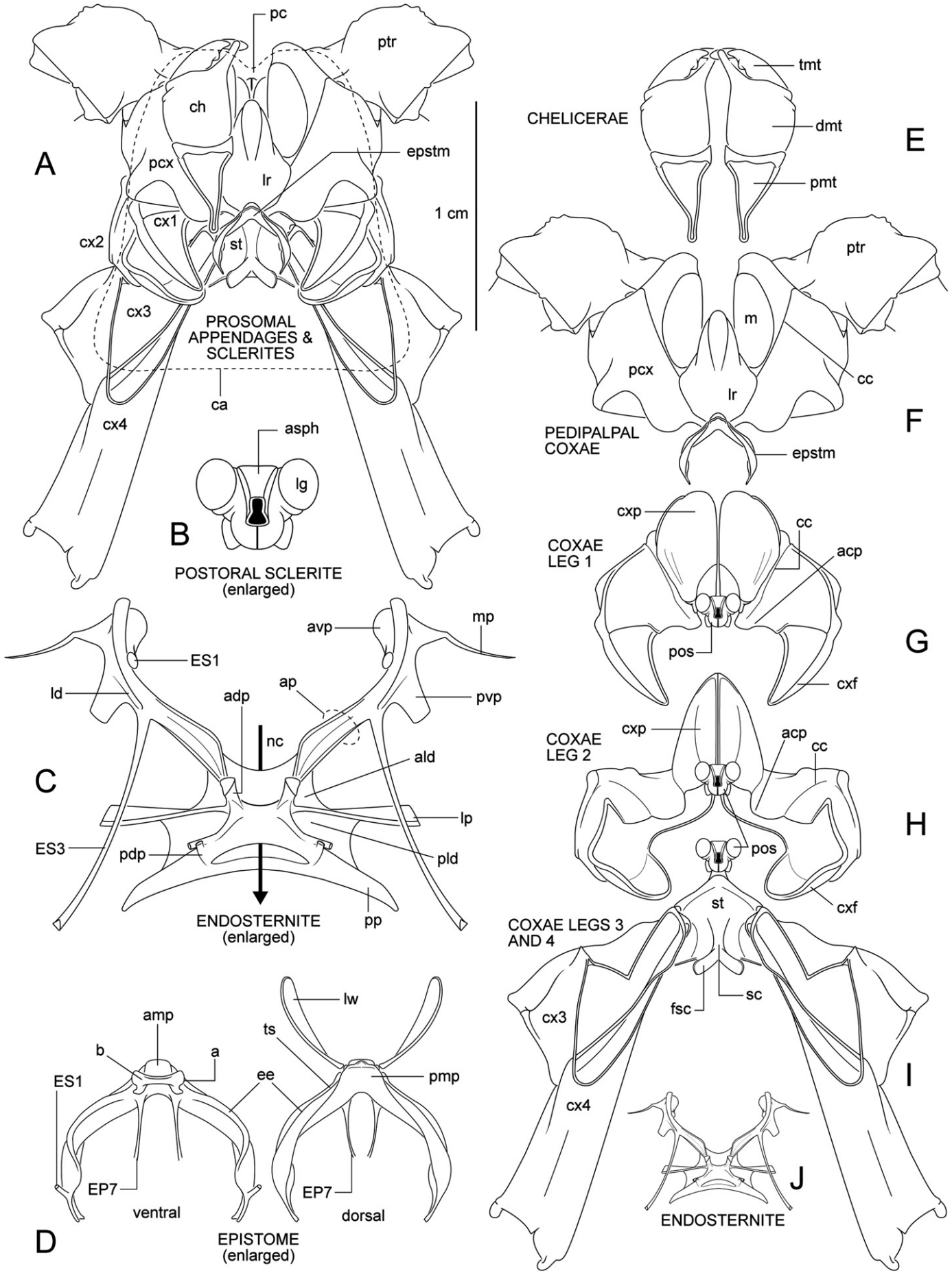
A
pc
ptr
ch
pcx
lr
epstm
cx1
cx2
st
cx3
cx4
1 cm
PROSOMAL
APPENDAGES &
SCLERITES
ca
B
asph
lg
POSTORAL SCLERITE
(enlarged)
C
avp
mp
ES1
ld
adp
ap
pvp
nc
ald
lp
ES3
pdp
pld
ENDOSTERNITE
(enlarged)
pp
D
lw
amp
ts
b
a
ES1
ee
pmp
EP7
ventral
EP7
dorsal
EPISTOME
(enlarged)
E
CHELICERAE
tmt
dmt
pmt
F
ptr
m
pcx
cc
lr
PEDIPALPAL
COXAE
epstm
G
cxp
cc
COXAE
LEG 1
acp
pos
cxf
H
cxp
acp
COXAE
LEG 2
cc
pos
cxf
st
I
COXAE LEGS 3
AND 4
fsc
sc
cx3
cx4
J
ENDOSTERNITE

posteriorly into the prosoma from the body of the epistome. They are invaginations of the cuticle but the lumen is largely obliterated by lateral compression and so appears in cross section to be formed by two cuticular layers.

The labrum–epistome complex of scorpions retains the muscles of the presumed primitive condition described above. A massive transverse muscle (Fig. 4B: *EP5*) attaches to the internal surfaces of the lateral walls of the epistome and, given the fusion of the latter with the pedipalpal coxae, contraction of *EP5* should cause powerful adduction of the coxae and compression of the preoral cavity. The anterior dorsoventral muscle of the labrum–epistome (*EP6*) attaches to the anteromedian and ventromedial surfaces of the labrum. Epistomal dilators of the pharynx arise from the ventral surface of the epistomal body (*PH4*) and the posterior median process (Fig. 4B: *PH3*).

The scorpion epistome departs radically from that of other chelicerates in having 14 pairs of muscles and ligaments in addition to those already described. Two pairs of muscles attach to the basal segment of the chelicera (Figs. 4A, 5D: *C7, C8*), two pairs attach to the pedipalpal coxae (Figs. 4B, 5D: *P4, P5*), four pairs attach to the carapace (Figs. 4B,C, 5D: *EP1–4*), one pair attaches to the body of the endosternite (Fig. 4B: *ES2*) and one pair attaches to the lateral walls of the precerebral pharynx (Figs. 4B, 5D: *PH7*). A pair of thin ligaments connects the body of the epistome to the pedipalpal coxae and postoral sclerite (Figs. 2D, 3A: *EP7*) and a pair of thick, tough ligaments connects the ventral surface of each epistomal entapophysis to the anterior process of the endosternite (Figs. 2C, 3A, 4B: *ES1*).

3.3. Sternites and subneural connective system

3.3.1. Sternites

The external anatomy of the ventral surface of the scorpion prosoma is well known, but there are few descriptions of its internal structure. The ventral non-appendicular body wall has two sclerites, the anterior postoral sclerite (Fig. 2B,G–I: *pos*) and posterior sternum (Figs. 2A,I, 3A: *st*). The postoral sclerite cannot be seen externally in intact animals and, as a consequence, is rarely mentioned even in technical surveys of scorpion anatomy. However, the structure is pivotal (both literally and figuratively) to the construction of the preoral chamber. The postoral sclerite is a heavily sclerotized mass, and the site at which the pedipalps and first two pairs of legs articulate with the body. The medial posterior (ventral) margin of the pedipalpal coxae articulates loosely with the postoral sclerite through thick but flexible ligaments. The dorsal surface of the sclerite has a pair of prominent rounded processes devoted to this ligamentous attachment (Fig. 2B: *lg*). The medial anterior (dorsal) margin of the coxa of leg 1 also articulates with the sclerite via flexible ligaments, but freedom of motion is not as great as in the pedipalpal coxae. The medial posterior (ventral) margin of the coxa of leg 1 fuses directly to the lateral surface of the sclerite, and mobility in this region is due entirely to the flexibility of the thin coxal cuticle. The medial anterior margin of the coxa of leg 2 has the same sort of fused connection. The medial posterior margins of pedal coxa 2 run in parallel down the center of the animal with the postoral sclerite lying above them and binding the two coxae firmly together (Fig. 2H). Thus, the appendicular articulations with the postoral sclerite have decreasing mobility in anterior-to-posterior sequence, with pedal coxae 2 being essentially immobilized with respect to the body.

The postoral sclerite is also intimately involved in the structure of the mouth and anterior end of the digestive tract. The mouth is a remarkably small opening on the anterior face of the postoral sclerite, which forms the posterior wall of the preoral chamber. The thin ascending pharynx is firmly attached to the anterior surface of the postoral sclerite as it passes dorsally and posteriorly (Fig. 2B: *asph*). The pharynx then arches posteriorly over the dorsal surface of the postoral sclerite and then continues into the hemocoel to join the greatly enlarged portion of the precerebral pharynx.

3.3.2. Subneural connective system

The ventral connective system of scorpions is described here for the first time. It consists of anterior and posterior sheets of connective tissue (subneural plastrons) and a metameric series of tendinous cords, or subneural connectives, that project laterally to attach to coxal margins of the postcheliceral appendages (Fig. 3A). Here the connectives receive fibers and/or connective tissue from the epistome (*EP7*) or endosternite (*ES10*). *ES10* is almost always closely associated with a member of the *L4* series of extrinsic coxal muscles.

The anterior subneural plastron (Fig. 3A: *asnp*) covers the internal surface of the postoral sclerite and has three pairs of subneural connectives. The first (anterior-most) connective

Fig. 2. Basic skeletal elements of the prosoma of *Heterometrus spinifer* from dorsal perspective. Scale bar applies to A and E–J. Abbreviations: *a*, articulation between epistome and pedipalpal coxa; *acp*, anterior coxal process; *adp*, anterior dorsal process of endosternite; *ald*, anterior lateral depression of endosternite; *amp*, anterior median process of epistome; *ap*, anterior process of endosternite; *asph*, ascending portion of precerebral pharynx; *avp*, anteroventral projection of endosternite; *b*, body of epistome; *ca*, carapace (marginal outline); *cc*, sulcus of *costa coxalis* indicating morphologically anterior surface of coxa; *ch*, chelicera; *cx1–cx4*, coxa of leg 1 to coxa of leg 4; *cxf*, posterior coxal flange; *cxp*, coxapophysis; *dmt*, deutomerite; *ee*, epistomal entapophysis; *EP7*, epistome-coxa ligament (see Table 1); *epstm*, epistome; *ES1*, cut end, endosternite-epistome ligament (see Table 1); *ES3*, anterior endosternite-carapace muscle (see Table 1); *fsc*, furca of sternal carina; *ld*, lateral depression of anterior process of endosternite; *lg*, point at which articular ligament of pedipalp attaches to postoral sclerite; *lp*, lateral process of endosternite; *lr*, labrum; *lw*, lateral wall of epistome; *m*, membrane of pedipalpal coxa; *mp*, marginal projection of endosternite; *nc*, path of ventral nerve cord through endosternite; *pc*, preoral chamber; *pcx*, pedipalpal coxa; *pdp*, posterior dorsal process of endosternite; *pld*, posterior lateral depression of endosternite; *pmp*, posterior median process of epistome; *pmt*, protomerite; *pos*, postoral sclerite; *pp*, posterior process of endosternite; *ptr*, pedipalpal trochanter; *pvp*, posteroventral projection; *sc*, sternal carina; *st*, sternum; *tmt*, tritomerite; *ts*, transverse sulcus of epistome.

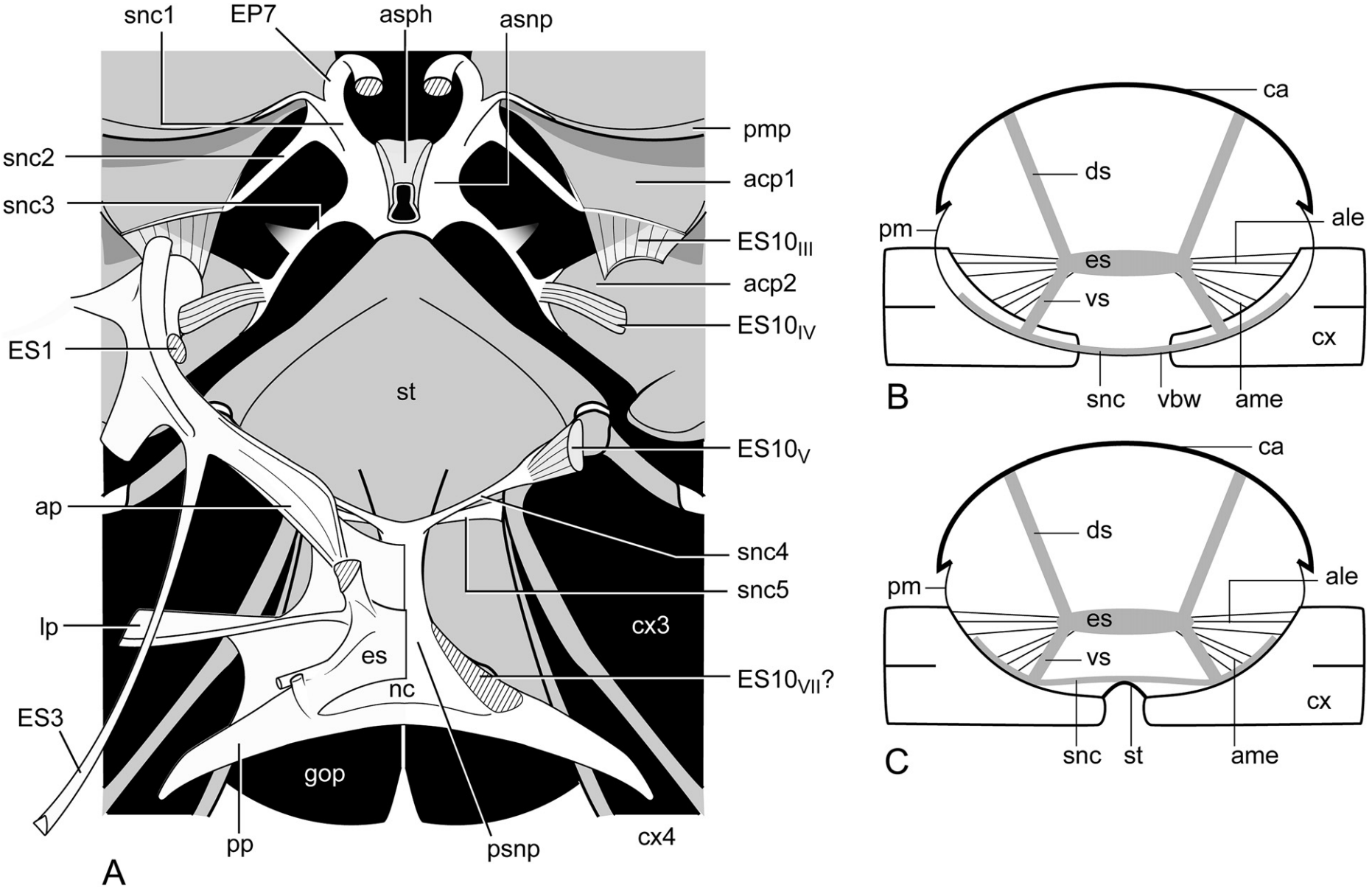

Fig. 3. Subneural connective system. (A) Diagrammatic view of medial intercoxal region of *Heterometrus spinifer* from dorsal perspective showing arrangement of subneural connective system (*asnp, psnp, snc1−5*) relative to the coxae (*cx*) and endosternite (*es*). Right side of endosternite and most muscles removed. (B) Diagrammatic cross section through hypothetical primitive (*Limulus*-like) arachnid showing primitive arrangement of subneural connective system. Subneural connectives (*snc*) adhere transversely to the ventral body wall (based on Shultz, 2001). (C) Diagrammatic cross section through a generalized scorpion showing arrangement of subneural connective system. Enlarged coxae (*cx*) replace the ventral body wall laterally and receive the subneural connectives (*snc*) from the sternum (*st*). Note that the subneural connectives are suspended in the hemocoel between the sternum and coxae (compare with A). Abbreviations: *acp1*, *acp2*, anterior coxal process of legs 1 and 2; *ale*, anterior lateral endosternite-coxa muscle; *ame*, anterior medial endosternite-coxa muscle; *ap*, anterior process of endosternite; *asnp*, anterior subneural plastron; *asph*, ascending pharynx; *ca*, carapace; *cx*, coxa; *ds*, dorsal endosternal suspensor muscle; *es*, endosternite; *gop*, genital operculum; *lp*, lateral process of endosternite; *nc*, neural canal; *pm*, pleural membrane; *pmp*, posterior (ventral) margin of pedipalpal coxa; *pp*, posterior process of endosternite; *psnp*, posterior subneural plastron; *snc1−5*, subneural connectives 1−5; *st*, sternum; *vbw*, ventral body wall; *vs*, ventral endosternal suspensor. The following are described in Table 1: *EP7*, *ES1*, *ES3, ES10*.

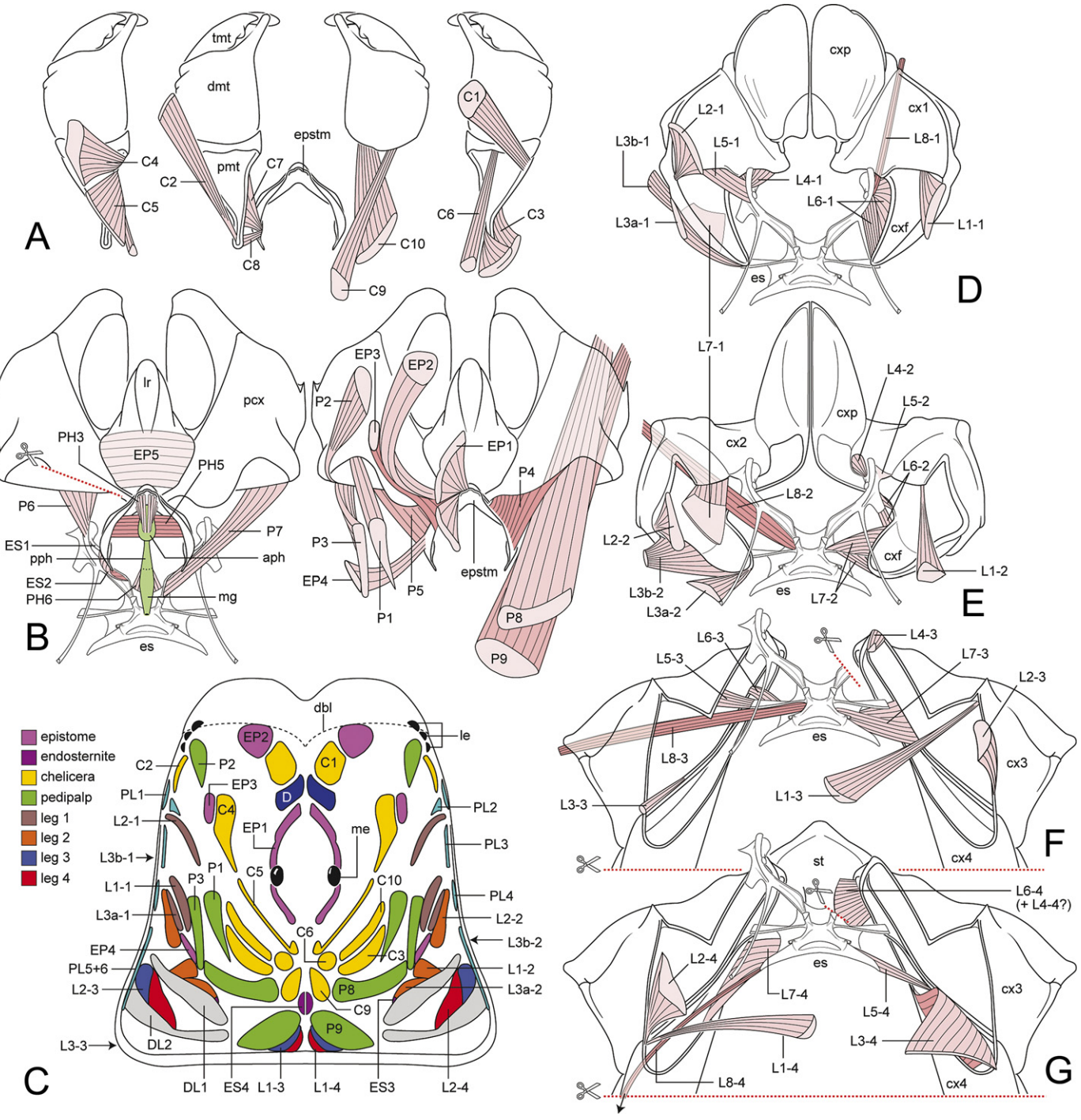

Fig. 4. Prosomal muscles of *Heterometrus spinifer*. All figures drawn from dorsal perspective at same scale. (A) Chelicerae; (B) pedipalpal coxae, epistome and pharynx; (C) carapace; (D) coxae of leg 1; (E) coxae of leg 2; (F) coxae of leg 3; (G) coxae of leg 4 and sternum. Arrows in C indicate approximate sites of muscle attachment on pleural membrane. Abbreviations beginning with capital letters are described in Table 1. Other abbreviations: *aph*, anterior or precerebral pharynx; *cx1–4*, pedal coxae 1–4; *cxf*, coxal flange; *cxp*, coxapophysis; *dbl*, posterior margin of anterior doublure of carapace; *dmt*, cheliceral deutomerite; *epstm*, epistome; *es*, endosternite; *le*, lateral eyes; *lr*, labrum; *me*, median eye; *mg*, midgut; *pcx*, pedipalpal coxa; *pmt*, cheliceral protomerite; *pph*, posterior or postcerebral pharynx; *st*, sternum; *tmt*, cheliceral tritomerite.

(Fig. 3A: *snc1*) passes dorsoanteriorly from the anterior margin of the subneural plastron and passes through the hemocoel to the pedipalpal coxa, where it attaches to the medial posterior (ventral) coxal margins and sends adherent marginal extensions both laterally and anteriorly. However, the main axis of the connective (Figs. 2D, 3A: *EP7*) continues dorsally through the hemocoel and terminates at a firm attachment to the ventral surface of the body of the epistome. The second connective (Fig. 3A: *snc2*) leaves the lateral margin of the anterior subneural plastron, passes laterally through the

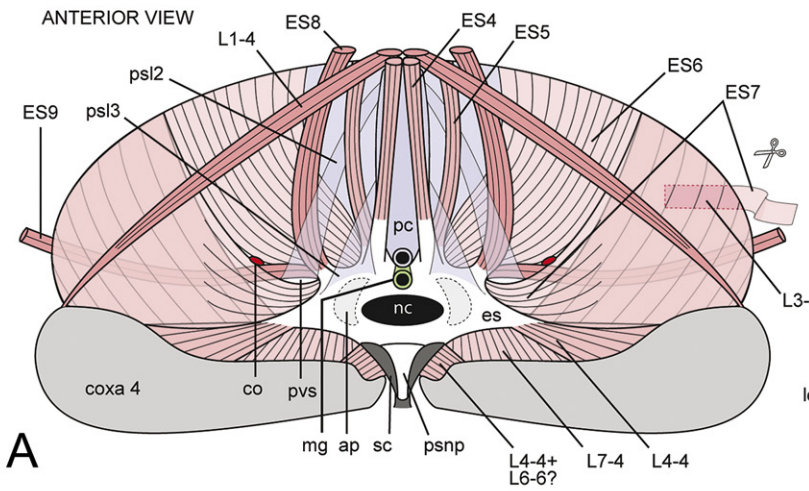

A

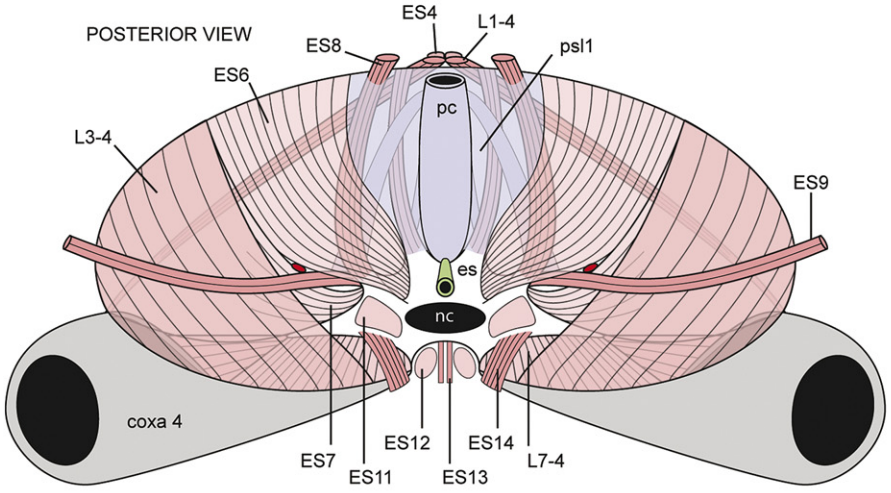

B

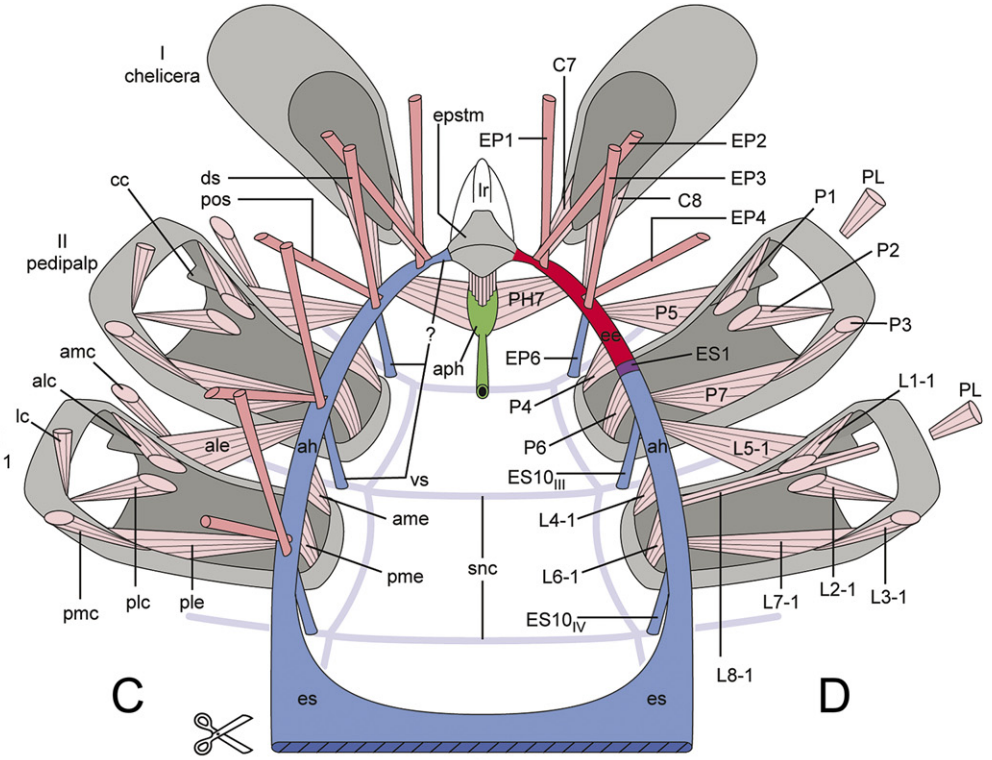

Euchelicerate Groundplan | "Undistorted" Scorpion Groundplan

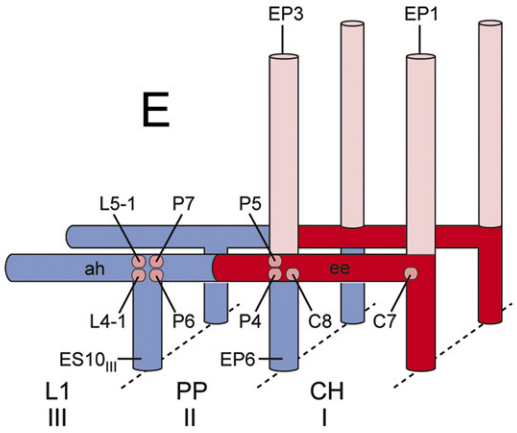

hemocoel for a short distance, and attaches to the medial anterior margin of the coxa of leg 1. Here again, adherent extensions pass medially and laterally along the coxal margin, with the lateral extension being longer. The lateral extension receives a thin sheet of muscle and connective tissue (Fig. 3A: $ES10_{III}$) from the end of the anterior process of the endosternite that appears superficially to form the ventral surface of muscle *L4-1* (Fig. 4D). The third connective (Fig. 3A: *snc3*) arises from the posterolateral margin of the subneural plastron and spans the hemocoel dorsolaterally toward the medial anterior margin of the coxa of leg 2. It receives a connective from the medial anterior coxal margin, but its main axis continues to the tip of the anterior coxal process of leg 2 (Fig. 3A: *acp*). It attaches and divides to form medial and lateral adherent extensions that run along the margin of the process. The medial extension receives muscles and connective tissue (Fig. 3A: $ES10_{IV}$) from the lateral medial surface of the anterior process of the endosternite just ventral to the ligament connecting the endosternite to the epistomal entapophysis (Fig. 3A: *ES1*). $ES10_{IV}$ appears to form the medial surface of muscle *L4-2* (Fig. 4E).

The posterior subneural plastron (Figs. 3A, 5A: *psnp*) adheres to the dorsal surface of the sternal carina (Fig. 2I: *sc*) and also spans the posterior furca of the sternal carina (Fig. 2I: *fsc*). The posterior subneural plastron forms the floor of the neural canal of the endosternite (Figs. 2C, 3A, 5A,B: *nc*). Two pairs of subneural connectives extend from the anterior end of the plastron. The larger dorsal connective (Fig. 3A: *snc4*) projects laterally into the hemocoel and attaches to the fused margins of the coxae of legs 3 and 4. It adheres broadly to the dorsal anterior margin of coxa 3 and continues laterally. It receives connective tissue and muscle fibers (Fig. 3A: $ES10_V$) from the ventral surface of the endosternite opposite the attachment of the anterior endosternite-carapace muscle (Fig. 3A: *ES3*). $ES10_V$ superficially appears to form the medial surface of muscle *L4-3* (Fig. 4F). The smaller ventral connective (Fig. 3A: *snc5*) splits from the dorsal cord near their attachment to the subneural plastron, passes ventrolaterally, and attaches to the proximal posterior margin of coxa 4. It differs from the other members in this series in lacking an intimate connection to a muscle attaching to the endosternite. The posterolateral margins of the posterior subneural plastron are continuous with the posterior surface of the endosternite and together the subneural plastron and endosternite form a complete circumneural ring (Figs. 2C, 3A, 5A,B).

3.4. Endosternite and diaphragm

3.4.1. Endosternite

The scorpion endosternite (Figs. 1C,J, 2, 3B,D–G: *es*) has been described by several authors, most notably Lankester et al. (1885). Details differ among workers, probably because some examined the endosternite *in situ* and others described it after removing it from the animal. The endosternites of the scorpions dissected here were examined *in situ* and were found to be very similar to one another.

The posterior surface of the endosternite is a roughly triangular plate with a broad ventral base and narrow dorsal apex (Figs. 2C, 3A, 4B). The posterior face slopes anterodorsally with the large neural canal (*nc*) opening at its center. The basal angles of the triangle are elongated into a pair of posterior processes (*pp*) and the median angle is crowned by a pair of anterior dorsal processes (*adp*), except in *Hadrurus* and related taxa (Pocock, 1902). A much smaller pair of posterior dorsal processes (*pdp*) extends from the sides of the triangle about midway between the anterior dorsal process and tip of the posterior process. A vertical sheet of connective tissue, the lateral process (Figs. 2C, 3A: *lp*), attaches to the endosternite at the base of each anterior dorsal process, and the resulting space between the lateral and posterior processes is spanned by a stiff, concave 'webbing' of connective tissue that forms the posterior lateral depression (Fig. 2C: *pld*). A pair of large anterior processes (Figs. 2C, 3A: *ap*) also attaches at the base of the anterior dorsal process. The space between the two anterior processes and between each ipsilateral anterior and lateral process is spanned by a sheet of connective tissue, the latter forming the anterior lateral depression (Fig. 2C: *ald*).

The anterior process is complex at its anterior end (Figs. 2C, 3A: *ap*). The sub-vertical stacking of the pedipalpal coxae and pedal coxae 1 and 2 noted above is reflected in this region of the endosternite. Extrinsic muscles of the pedipalps and leg 1 tend to attach to a longitudinal dorsal projection of the anterior process and those of leg 2 tend to attach ventral to these (Fig. 4B,D,E). The anterior end of the anterior process is anchored firmly to the dorsoanterior surface of the coxa of leg 2, and an adherent process of connective tissue (Fig. 2C: *mp*) passes laterally along the anterior margin of the coxa. A thin anterior endosternite-carapace muscle (Figs. 2C, 3A: *ES3*) arises from the dorsal surface of the anterior process; it has been overlooked by most workers (except Pocock, 1902). Finally, the anterior process is connected to the ventral

Fig. 5. Endoskeleton of scorpions. (A, B) Diaphragm of *Heterometrus spinifer* (semi-diagrammatic). (C–E) Hypothesis for evolution of epistomal entapophysis. (C, D) Comparison between anterior endosternal horn of the euchelicerate groundplan (C) and epistomal entapophysis of scorpions (D) [diagrammatic, first three postoral segments, nervous system and midgut removed, dorsoposterior perspective]. See Fig. 6 for another depiction of the arachnid and scorpion groundplans and Fig. 4 for more literal depictions of scorpion morphology. Abbreviations beginning with capital letters are described in Table 1. Other abbreviations: *I–III*, postoral segments I–III; *ah*, anterior horn of endosternite; *alc*, anterolateral carapace-coxa muscle; *ale*, anterolateral endosternite-coxa muscle; *amc*, anteromedial carapace-coxa muscle; *ame*, anteromedial endosternite-coxa muscle; *ap*, base of anterior process of endosternite (cut); *aph*, anterior or precerebral pharynx; *cc*, *costa coxalis*; *co*, passage connecting coxal organ (prosomal side) and lateral lymphoid organ (opisthosomal side) (not present in Buthidae); *ds*, dorsal endosternal suspensor; *ee*, epistomal entapophysis; *epstm*, epistome; *es*, endosternite; *lc*, lateral carapace-coxal muscle; *lr*, labrum; *mg*, midgut; *nc*, neural canal; *pc*, pericardium; *plc*, posterolateral carapace-coxa muscle; *ple*, posterolateral endosternite-coxa muscle; *pmc*, posteromedial carapace-coxa muscle; *pme*, posteromedial endosternite-coxa muscle; *pos*, posterior oblique endosternal suspensor; *psl1–3*, pericardial suspensory ligaments 1–3; *psnp*, posterior subneural plastron; *pvs*, passage of venous sinus; *sc*, sternal carina; *snc*, subneural connectives; *vs*, ventral endosternal suspensor.

surface of the epistomal entapophyses by a pair of tough ligaments (Figs. 2C, 3A: *ES1*).

The posterior face of the endosternite (Fig. 5B) has several muscles that pass into the opisthosoma. Paired ventral longitudinal muscles arise on either side of the neural canal (Fig. 5B: *ES11*) and posterior margin of the sternal carina (Fig.4: *ES12*), pass posteriorly and attach to the pectinal chondrite. Another pair of muscles extends from the base of the posterior process of the endosternite (Fig. 5B: *ES14*) to the anterolateral margin of the pecten. Finally a pair of small muscles passes from the ventral margin of the endosternite to the genital operculum (Fig. 5B: *ES13*).

3.4.2. Diaphragm

The scorpion diaphragm is often described as a near-vertical sheet of muscle associated with the posterior end of the endosternite that divides the hemocoel into distinct prosomal and opisthosomal compartments (Lankester et al., 1885; Pocock, 1902; Firstman, 1973; Farley, 1999). This characterization is largely accurate but ignores the diaphragm's intrinsic complexity and composite structure.

The dorsomedial portion of the diaphragm is formed primarily by the pericardium (Fig. 5A,B: *pc*) and its associated membranous ligaments, but there are also four pairs of strap-like muscles, two medial pairs (*ES4, ES5*) and two lateral pairs (*ES8, ES9*). *ES4* (Figs. 4C, 5A,B) arises from the anterior dorsal process and inserts on the posterior median surface of the carapace. It projects dorsally from the endosternite at the anterior margin of the diaphragm but is not actually a part of it. *ES4* is absent in *Hadrurus*. *ES5* also arises from the anterior dorsal process, passes dorsoposteriorly along the anterior surface of the diaphragm just lateral to the pericardium, and attaches to a transverse bar of connective tissue connected to the anterior margin of the first opisthosomal tergite. *ES8* arises from the posterior dorsal process of the endosternite (Fig. 2C: *pdp*), passes dorsad along the anterior surface of the diaphragm, penetrates the diaphragm dorsally, and inserts on the anterior surface of the first opisthosomal tergite (Fig. 5A,B). An extremely long, thin muscle (Fig. 5A,B: *ES9*) originates from the anterior surface of the posterior dorsal process, passes posterolaterally through a fenestra in the diaphragm and continues laterally along the posterior surface of the diaphragm. The muscle attaches to the anterolateral margin of the second opisthosomal tergite.

The lateral sector of the diaphragm is formed primarily by an extrinsic leg muscle, *L3-4*, that arises along the distal half of the posterior margin of coxa 4 and inserts along the transverse connective bar of tergite 1 (Figs. 4G, 5A,B). A second extrinsic muscle, *L7-4*, completes the ventral sector of the diaphragm. *L7-4* arises along the proximal half of the posterior margin and inserts on the ventral surface of the posterior process of the endosternite.

The large dorsolateral sector between the pericardial membranes and *L3-4* is filled primarily by two broad, sheet-like muscles (Fig. 5A,B: *ES6, ES7*), both of which arise between the anterior and posterior dorsal processes of the endosternite and insert along the transverse connective bar of tergite 1. *ES6* lies medial to *ES7* and is composed primarily of muscle fibers, but *ES7* is muscular basally and becomes a membranous tendon as it overlaps the anterior surface of *L3-4*. The lateral margin of *ES6* and medial margin *ES7* are firmly attached, except near their origin at the endosternite where they separate and form a passage or fenestra through the diaphragm. *ES9* (described above) passes through the fenestra and divides it into dorsal and ventral sections. The coxal gland of the prosoma communicates with the lateral lymphoid organ of the opisthosoma through the dorsal section and the venous sinus passes through the ventral section. The lymphoid organ is absent in *Centruroides* and other buthids and thus a dorsal passage is lacking.

Membranous ligaments associated with the pericardium form much of the dorsal medial portion of the diaphragm but also extend over its surfaces and appear to integrate the diaphragmatic muscles into a near-continuous sheet. Three ligamentous structures are evident. The main suspensory ligament of the pericardium (Fig. 5B: *psl1*) appears to span the entire anterior surface of the diaphragm, attaching to the dorsal transverse tendon of tergite 1, the posterior process of the endosternite, and the posterior margin of coxa 4. Another ligament (Fig. 5A: *psl2*) separates dorsally from the suspensory ligament and passes ventrally lateral to the pericardium. A portion of this ligament enters the fenestra of the diaphragm and reinforces its dorsal margin. A third ligament (Fig. 5A: *psl3*) arises broadly from the lateral surface of the pericardium, passes anteriorly between *ES4* ad *ES5* (thereby binding *ES5* to the dorsal surface of the diaphragm) and attaches to the endosternite. A complex of ligaments also extends into the prosoma, but it is not part of the diaphragm and was not examined in detail.

3.5. Foregut

The cuticle-lined foregut, or stomodeum, of chelicerates consists of a well-developed precerebral pharynx, a transcerebral esophagus and a variably developed postcerebral pharynx. The precerebral pharynx in scorpions is comprised largely of a muscularized chamber (Fig. 4B: *aph*) that resembles an inverted triangle in cross section, with two long lateral walls and a short dorsal wall. It receives imbibed fluid through a narrow ascending pharynx (Figs. 2B, 3A: *asph*). The precerebral pharynx is equipped with dorsal and lateral constrictor muscles (*PH1, PH2*) and dorsal dilators arising from the body of the epistome (*PH5*), posterior median process of the epistome (Fig. 4B: *PH4*) and intercheliceral septum (*PH3*). Large lateral dilators originate from the medial walls of the epistomal entapophyses (Fig. 4B: *PH7*). The esophagus is a short tube without extrinsic muscles that exits the precerebral pharynx ventrally and passes posteriorly between the supra- and subesophageal ganglia. The postcerebral pharynx (Fig. 4B: *pph*) is broader than the esophagus and receives the apex of a triangular sheet of muscle that arises broadly form the anterior margin of the endosternite (Fig. 4B: *PH9*). The postcerebral pharynx merges with the midgut (Fig. 5A: *mg*), which passes posteriorly between the pericardium and dorsal surface of the endosternite.

4. Discussion

4.1. Background: The box-truss axial system of arthropods, especially arachnids

An appreciation of the primitive axial endoskeletal system of arthropods (Figs. 1D,E, 6) is important for understanding skeletomuscular evolution in scorpions and the mesoderm-template hypothesis (Fig. 1E). Comparisons among crustaceans, myriapods, hexapods, chelicerates and trilobites indicate that basal members of extant arthropod lineages share a fundamental arrangement of axial muscles and connective endoskeletal elements (Cisne, 1974, 1981; Boudreaux, 1979; Fanenbruck, 2003). Its main components are a pair of ventral longitudinal connectives (Figs. 1D,E, 6: *lc*), that run the length of the body. The longitudinal connectives attach to each other

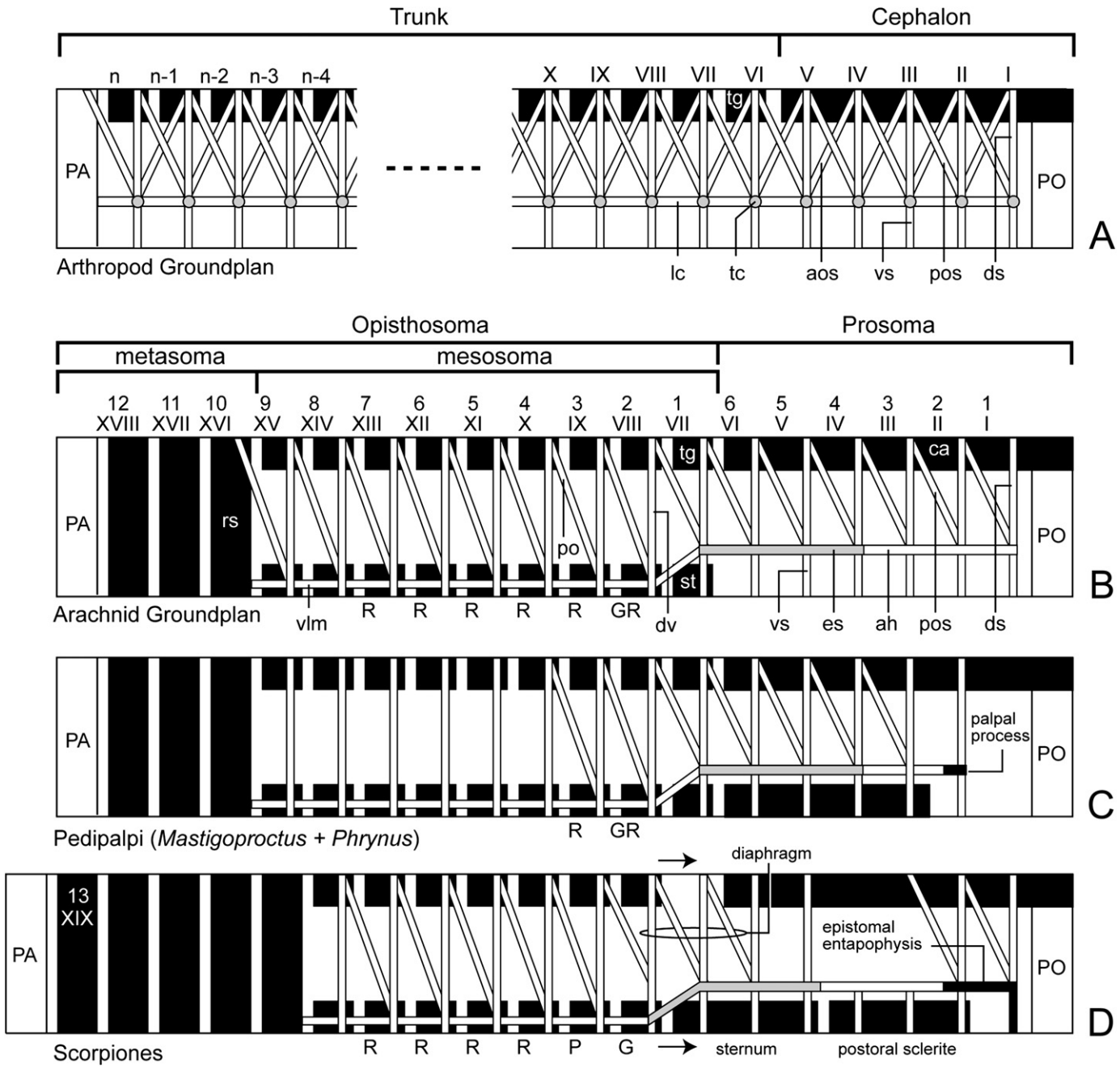

Fig. 6. Diagrammatic medial perspectives of representative endoskeletal systems showing correspondence between epistomal entapophyses and diaphragm of scorpions to axial components of other arthropods. (A) Arthropod groundplan; (B) Euchelicerate groundplan; (C) Pedipalpi; (D) Scorpiones. Arrows indicate displacement of segments. Based on Shultz (1991, 1993, 1999) and the present study. Abbreviations: *ah*, anterior horn of endosternite; *aos*, anterior oblique suspensor; *ca*, carapace; *ds*, dorsal suspensor; *dv*, dorsoventral muscle; *es*, endosternite; *G*, genital segment; *lc*, longitudinal connective; *P*, pectines; *PA*, postanal or non-segmental perianal structures; *PO*, preoral structures; *po*, posterior oblique muscle; *pos*, posterior oblique suspensor; *R*, segment with appendage-derived respiratory lamellae; *rs*, ring sclerite (sternite and tergite fused); *st*, sternite; *tc*, transverse connective; *tg*, tergite; *vlm*, ventral longitudinal muscle; *vs*, ventral suspensor.

at each segmental juncture through a transverse connective (Fig. 1D,E, 6A: *tc*). The lateral end of each transverse connective is attached to the ventrally adjacent body wall by paired ventral suspensors (*vs*), to the dorsally adjacent tergite by dorsal suspensors (*ds*), to the tergite of the anteriorly adjacent segment by anterior oblique suspensors and to the posteriorly adjacent tergite via posterior oblique suspensors (*pos*) (Figs. 1D, 6A). The resulting system resembles a box truss in lateral perspective and has been termed the box-truss axial muscle system (BTAMS) by Shultz (2001) (see also Fanenbruck, 2003). The BTAMS serves as a mechanically dynamic endoskeleton to which extrinsic appendicular and pharyngeal muscles attach (Fig. 1D,E).

The extant euchelicerates depart from the hypothetical primitive BTAMS in several respects (Fig. 6B). Most significantly, the ventral longitudinal connectives spanning postoral segments I–VII and transverse connectives of segments IV–VII have 'tendonized' to form an endosternite, a roughly horizontal sheet of cartilage-like connective tissue suspended in the prosomal hemocoel by a metameric series of muscles (Fig. 6B: *es*) (Firstman, 1973). These muscles include the paired dorsal, posterior oblique and ventral suspensors (Figs. 5C, 6B: *ds, pos, vs*); the anterior oblique suspensors are absent. The endosternite receives pharyngeal (Fig. 5C) and extrinsic appendicular muscles (Fig. 5C: *ame, ale, pme, ple*). The anterior oblique muscles of the post-endosternal BTAMS are absent in arachnids (but present in Xiphosura) (Shultz, 2001), and the posterior oblique suspensors tend to be retained only in those opisthosomal segments with significant appendicular elements, such as book lungs, gonopods, spinnerets and pectines.

4.2. The 'pregenital compression' hypothesis for evolution of the scorpion diaphragm

I hypothesize that the diaphragm was assembled during evolution mainly through the longitudinal reduction of the first opisthosomal segment, a transformation that brought muscles of segments VI through VIII into close proximity and facilitated their integration into a nearly continuous barrier (Fig. 6D). During this process, external indications of the first opisthosomal segment (segment VII) were largely eliminated, an evolutionary transformation that is apparently recapitulated during ontogeny (Brauer, 1895) as the 'transient' pregenital segment. Those muscles one would expected to attach to tergite VII based on the arachnid groundplan have shifted to a large dorsal transverse tendon fused to the anterior margin of the tergite VIII, which is now the first apparent tergite of the opisthosoma. The observations and arguments used in formulating this hypothesis are summarized below.

The dorsal and posterior oblique suspensor muscles of segments VI through VIII (i.e., *ES4–ES9*) can be readily distinguished within the structure of the diaphragm (Fig. 5A,B). Those of segment VI, the last prosomal segment, arise from the anterior dorsal process of the endosternite. As expected, the dorsal suspensor (*ES4*) attaches dorsally to the carapace and the posterior oblique suspensor (*ES5*) attaches dorsally to the posteriorly adjacent segment, which is represented by the dorsal transverse tendon of the first apparent tergite. The dorsal and posterior oblique suspensors of segment VII (*ES6, ES7*) also have a common endosternal attachment, the dorsoposterior margin of the endosternite between the anterior and posterior dorsal processes. Here, the dorsal attachments are also consistent with the hypothesis. Both attach to the dorsal transverse tendon, which represents both the dorsal surface of segment VII and segment VIII. Finally, the dorsal and posterior oblique suspensors of segment VIII, the genital segment, arise ventrally from the posterior dorsal process of the endosternite. The dorsal suspensor (*ES8*) attaches to the first apparent tergite and the posterior oblique suspensor (*ES9*) passes rearward and inserts on the following (pectinal) tergite (IX). The dorsal and posterior oblique muscles of the remaining mesosomal segments continue this pattern of on intra- and intersegmental attachment, respectively.

The remaining muscular components of the diaphragm attach ventrally to the coxa of leg 4 (Fig. 5A,B). One large sheet-like muscle (*L3-4*) with vertically arranged fibers completes the lateral portion of the diaphragm. There is a metameric homolog of this muscle in the other legs and all appear to correspond to the posterior lateral carapace-coxa muscle of the arachnid groundplan. The other extrinsic leg muscle (*L7-4*) completes the ventral sector of the diaphragm. It attaches along the posterior margin of the coxa and to the ventral surface of the posterior process of the endosternite. Again, this muscle corresponds to similar muscles in the other legs (i.e., *L7*) and represents the posterior lateral endosternite-coxa muscle of the arachnid groundplan (Fig. 5C: *ple*).

The pericardiac ligaments that complete the anterior medial portion of the diaphragm are also consistent with the pregenital reduction hypothesis. Xiphosurans and pulmonate arachnids have a metameric series of ligaments that attach to the pericardium. Typically, lateral ligaments connect the pericardium to the dorsal body wall within each segment and a ventral pair connects the pericardium to the endosternite, respiratory venous sinus or ventral body wall depending on the position of the segment in the body. The ventral pericardial ligaments often have a muscular component, the veno-pericardiac muscles. Each ventral ligament passes anterior to the dorsal endosternal suspensor or dorsoventral muscle of the same segment as it passes from the pericardium to its ventral attachment. The main pericardial suspensory ligament (*sl1*) of the scorpion diaphragm appears to represent a greatly expanded lateral pericardial ligament of segment VII of other chelicerates, and ligaments *sl2* and *sl3* may correspond to the ventral pericardial ligaments of segments VIII and VII, respectively.

The pregenital compression hypothesis accommodates most aspects of diaphragm morphology, but not all. Specifically, the apparent dorsal endosternal suspensor of segment VII (Fig. 5A,B: *ES6*) passes posterior rather than anterior to the dorsal suspensor of segment VIII (*ES8*) and the posterior oblique suspensor of segment VII (*ES7*) passes anterior rather than posterior to the extrinsic leg muscle *L3* of leg 4 (*L3-4*). Thus, the anterior-posterior sequence of ventral attachments of the endosternal muscles is consistent with the pregenital

compression hypothesis, but this is not strictly the case for the dorsal attachments. It is possible that the order of dorsal attachments is influenced by relative timing or orientation of muscle growth, differentiation or attachment during development. Furthermore, pregenital reduction does not explain the apparent incorporation of axial muscles of segment VIII, the genital segment, into the endosternite, which typically ends in segment VII.

The size and complexity of the diaphragm suggest it has an important role. Several workers have speculated that it has some 'circulatory' function (Firstman, 1973; Hjelle, 1990); Farley (1999) suggests that it allows the prosomal and opisthosomal hemocoels to operate at different internal fluid pressures. Running spiders offer a precedent for this phenomenon, due largely to their use of hydraulic pressure in propulsive leg extension (Parry and Brown, 1959; Stewart and Martin, 1974; Anderson and Prestwich, 1975; Prestwich, 1988) and a narrow prosoma-opisthosoma junction. But scorpions rely on different methods of joint extension (Shultz, 1991; Sensenig and Shultz, 2003, 2004) and have a very broad prosoma–opisthosoma junction. Furthermore, the anatomy of the diaphragm is not consistent with this proposal. Its central portion is formed largely by a membranous ligament (Fig. 4: *psl1*), which seems poorly designed to enforce a pressure differential between the prosomal and opisthosomal compartments.

In contrast, I suggest that the diaphragm is a mechanical barrier that prevents intrusion of opisthosomal contents into the prosomal compartment during violent deformations of the opisthosoma associated with predatory or defensive stinging behavior. Aside from hemolymph, the opisthosomal hemocoel is filled primarily by midgut diverticula, although embryos can also occupy a substantial volume in females. Both diverticula and embryos, where present, press up against the posterior surface of the diaphragm. In the absence of a diaphragm, sudden reduction in volume or increase in pressure in the opisthosoma would tend to drive opisthosomal contents into the prosoma, where they could deform or compress the coxal organ, brain and optic nerves and interfere with the operation of appendages. Consequently, the diaphragm may be an important functional component of the stinging mechanism.

4.3. The mesoderm-template model for the evolutionary origin of the epistomal entapophyses in scorpions and cuticular endoskeletons in other arthropods

4.3.1. Evidence for the mesoderm-template model in scorpions

A recurring theme in the evolutionary morphology of the arthropod cephalon is the transition from a mesodermally derived connective endoskeleton (endosternite, pseudotentoria, etc.) to an endoskeleton with significant cuticular components (apodemes, tentoria, entapophyses, etc.) (Bitsch and Bitsch, 2002), an issue addressed most often in studies of the hexapod tentorium (e.g., Snodgrass, 1928, 1951, 1960; Manton, 1964; Koch, 2000). However, due to substantial variation in the gnathocephalon of basal hexapod lineages and uncertainties about the hexapod sister group, entomologists have yet to synthesize cephalic skeletomuscular anatomy across Hexapoda in sufficient detail to allow noncontroversial homologization of key endoskeletal elements or to offer specific evolutionary or developmental hypotheses to explain the connective-to-cuticular transition. Chelicerates have been largely omitted from the discussion but appear to be good candidates for addressing the topic, given the existence of a model of the prosomal groundplan (Figs. 5C, 6B) and a system for homologizing muscular and endoskeletal elements (Shultz, 1991, 2001).

Scorpions differ from most other chelicerates in having a well-developed cuticular endoskeleton, the epistomal entapophyses (Fig. 1D,F). In most chelicerates the epistome is a relatively simple structure equipped with a few muscles for operating the preoral chamber and precerebral pharynx, although the endosternite often terminates on or near its proximal margin (Snodgrass, 1948; Palmgren, 1978; Shultz, 2000, 2001). In scorpions, however, each epistomal entapophysis bears 14 extrinsic muscles, tendons and ligaments that attach to the chelicerae, pedipalps, endosternite and precerebral pharynx (Fig. 4A,B).

The scorpion epistomal complex would seem to be a major and complex evolutionary innovation, but comparison with the arachnid groundplan (Fig. 5C,D) suggests a simple explanation: the anterior epistomal attachment of the original mesodermal endoskeleton—or, more specifically, the embryological precursor to the mesodermal endoskeleton—signals the adjacent ectoderm to invaginate and then guides the resulting ectodermal tube into the embryonic endoskeleton to a point halfway through the pedipalpal segment (Fig. 5D,E). The muscles, tendons and ligaments that would normally have attached to the connective tissue endoskeleton, including the remainder of the mesodermal endoskeleton, now attach to the entapophysis. If correct, this process explains how positional homology could exist in two structures (i.e., connective and cuticular endoskeletons) that differ in developmental origin and material composition.

4.3.2. The mesoderm-template model and the embryonic extracellular matrix

I suggest that the positional information common to the connective and cuticular endoskeletons is provided by components of the embryonic extracellular matrix (ECM). The ECM in *Drosophila* and other animals performs many important developmental functions, such as mediating cell-cell and cell-matrix attachment (Umemiya et al., 1997), regulating cell migration, growth and proliferation (Garcia-Alonso et al., 1996; Kresse and Schönherr, 2001), and providing an embryonic skeleton (Sheetz et al., 1998). Gene products expressed within the ECM regulate ectoderm-mesoderm interactions, including proper formation of apodemes, tracheae and other cuticular structures as well as the differentiation and growth of muscles and their attachment to apodemes (Leptin et al., 1989; Adams and Watt, 1993; Umemiya et al., 1997; Vorbrüggen and Jäckle, 1997). The ECM is composed largely of glycoproteins (e.g., collagen) and proteoglycans (e.g. chrondroitin sulfate). It is reasonable to suppose that a spatially restricted component of the ECM is necessary for the assembly and differentiation

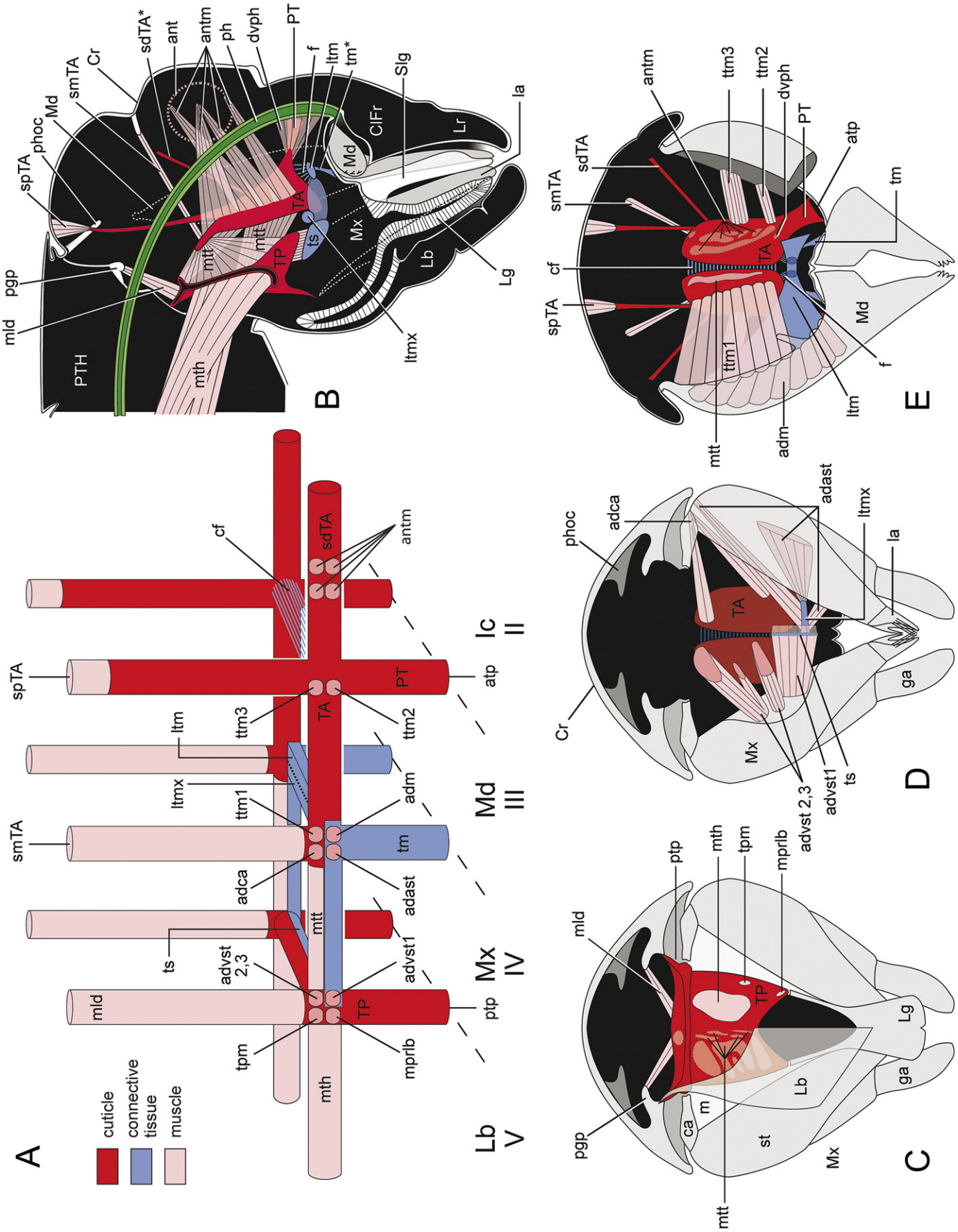
A
cuticle
connective tissue
muscle
Lb V
Mx IV
Md III
Ic II
spTA
smTA
mld
ts
advst 2,3
tpm
mth
cf
sdTA
antm
PT
atp
ltm
ttm3
TA
ttm2
ltmx
ttm1
adm
adca
tm
adast
mttt
advst1
TP
ptp
mprlb
B
PTH
mld
pgp
spTA
phoc
Md
smTA
Cr
sdTA*
ant
antm
ph
dvph
PT
f
ltm
tm*
Slg
ClFr
Lr
la
Lg
ltmx
Lb
Mx
ts
TA
mtt
TP
mth
C
mld
ptp
mth
tpm
mprlb
TP
Lg
Lb
ga
pgp
ca
m
st
Mx
mtt
D
phoc
adca
adast
ltmx
la
TA
Cr
Mx
ga
advst 2,3
advst1
ts
E
antm
ttm3
ttm2
dvph
PT
atp
sdTA
smTA
tm
cf
TA
spTA
Md
ttm1
f
mtt
adm
ltm

of the intersegmental tendon system of arthropods. In fact, given the similarity of the connective endoskeleton to the ECM in mechanical function, histology and material composition (Cole and Hall, 2004a,b), some components of the post-embryonic intersegmental tendon system may be persistent, hypertrophied elements of the ECM. Given the active roles played by the ECM in the development of the skeletomuscular system, it is possible that the ECM precursor to the intersegmental tendon system promotes and guides invagination of the ectoderm and thereby imposes its own spatial configuration on the resulting cuticular structures and mediates the attachment of muscles to it. This mechanism could explain the apparent 'replacement' of the connective endoskeletal elements by cuticular invaginations with the same shape and arrangement of muscle attachments in arthropods. Consequently, I have termed this the mesoderm-template model of ectodermal invagination.

4.3.3. Tentoria of Archaeognatha (Hexapoda) and Symphyla (Myriapoda) interpreted in light of the mesoderm-template model

The basic assumptions of the mesoderm-template model (Fig. 1E) are (1) ectodermal invaginations leading to cephalic apodemes are initiated at points where the embryological precursor to the mesodermal endoskeleton attach to the exoskeleton (i.e. dorsal or ventral suspensors); (2) the path followed by the ectodermal invagination is determined by the spatial limits imposed by the mesodermal endoskeleton, and (3) the relative positions of dorsal and ventral suspensors ($ds_{n/n+1}$, $vs_{n/n+1}$), longitudinal and transverse connectives (lc_n, $tc_{n/n+1}$), and extrinsic appendicular muscles (ale_n, ame_n, ple_n, pme_n) should be retained in the final endoskeleton, whether cuticular elements are incorporated or not. Using these principles, I have interpreted the cephalic endoskeletons of two relatively well-studied arthropods, archaeognathans and symphylans, to demonstrate the potential generality of the mesoderm-template model.

Archaeognatha. Several studies of the skeletomuscular anatomy of the archaeognathan head have been undertaken, notably Manton (1964) and Fanenbruck (2003), but that of Bitsch (1963) based on examination *Petrobius*, *Machilis* and *Dilta* is by far the most thorough and is thus relied upon here. All relevant muscles described by Bitsch are encompassed by this interpretation.

Interpretation (compare Figs. 1E, 7A): The anterior tentorium results from paired ectodermal invaginations initiated at the ventral suspensors at the junction of the intercalary and mandibular segments ($vs_{II/III}$), which are indicated externally by anterior tentorial pits (Fig. 7E: *atp*) (Larink, 1969). The ectodermal invagination eventually grows into the corresponding dorsal suspensor (ds_{III}) and adjacent longitudinal connectives ($lc_{I–III}$) and spans the head from the second transverse connective posteriorly ($tc_{III/IV}$) to the anterior end of the endoskeleton. The ectoderm does not enter either the first transverse connective ($ts_{II/III}$), which persists as connective fibers (Fig. 7A,E: *cf*), or the second transverse connective ($tc_{III/IV}$).

The 'cuticularized' premandibular longitudinal connectives (lc_I, lc_{II}) and, perhaps, ds_I persist in the adult as two fine processes (Fig. 7A,B,E: *sdTA*) (= 'dorsal tentorial arm' of Snodgrass, 1928) that have a non-muscular attachment to the cranium. [This structure was overlooked by Manton (1964).] This interpretation is consistent with embryological observations of the cockroach *Blatta* (Riley, 1904) which show that the dorsal tentorial arm is an ectodermal projection from the anterior tentorium, not an ingrowth from the cranium. It also provides a simple explanation for attachment of extrinsic antennal muscles on this structure in insects; that is, it is the primitive site of attachment, not a 'migration' of muscles from the cranium to an apomorphic apodeme, as proposed by Snodgrass (1928). The cuticular projection corresponding to $ds_{II/III}$ (Fig. 7A,B,E: *spTA*) attaches to the cranium via muscle. This interpretation is supported by its innervation from the mandibular ganglion (Bitsch, 1963) and a cranial attachment anteriorly adjacent to extrinsic mandibular muscles. Interestingly, Chaudonneret (1950) suggested that the apparently homologous structure in *Thermobia* (Thysanura) occupies the border between the intercalary and mandibular segments. The structure corresponding to $ds_{III/IV}$ (Fig. 7A,B,E: *smTA*) springs from the posterior dorsal margin of the tentorium and inserts on the cranium anterior to the compound eye. Its anterior cranial attachment is unexpected, but homology

Fig. 7. Cephalic endoskeleton of Archaeognatha (Hexapoda). (A) Hypothetical mesodermal template of the head endoskeleton showing proposed developmental fates of different components, where red is invaginated ectoderm (tentorium), blue is connective tissue and pink is muscle. Compare to Fig. 1E for proposed groundplan homologs. (B) Sagittal view of archaeognathan head (redrawn from Manton, 1964, modifications according to Bitsch, 1963 indicated with an asterisk). (C–E) Sequential cross sections of the head of an archaeognathan shown from posterior perspective (redrawn and modified from Bitsch, 1963). (C) Posterior view of cervical region showing posterior tentorium (*TP*). Left side of tentorium is transparent to show attachments of muscles on anterior surface. (D) Same view as C with labium and posterior tentorium removed. Left side shows posterior maxillary muscles. Right side shows anterior muscles through transparent posterior wall of maxilla. (E) Posterior view of transverse section taken anterior to those in C and D showing mandible and posterior surface of anterior tentoria. Left side shows posterior mandibular muscles and muscle attachments to the posterior tentorial surface. Right side shows anterior mandibular muscles; transparent anterior tentorium showing muscle attachments on anterior surface; section removed from mandible to show position of anterior tentorial pit (*atp*). Abbreviations largely follow Bitsch (1963): *II–V*, second to fifth postoral segments; *adast*, anterior adductor of stipes; *adca*, tentorial adductor of cardo; *adm*, mandibular adductor muscle; *advst*, ventral adductor of stipes; *ant*, internal margin of antenna; *antm*, antennal muscles; *atp*, anterior tentorial pit; *ca*, cardo; *cf*, intertentorial connective fibers; *ClFr*, clypeus-frons; *Cr*, cranium; *dvph*, ventral pharyngeal dilator muscle; *f*, fibrillar formation; *ga*, galea; *Ic*, intercalary (premandibular) segment; *la*, lacinia; *Lb*, labium; *Lg*, lingua (= posterior lobe of hypopharynx); *Lr*, labrum; *ltm*, mandibular tendon; *ltmx*, maxillary tendon; *m*, arthrodial membrane; *Md*, mandible; *mld*, dorsal muscle of labial segment; *mprlb*, prelabial muscle; *mth*, ventral longitudinal muscles from thorax; *mtt*, tentorio-tentorial muscle; *Mx*, maxilla; *pgp*, postgenal process; *ph*, pharynx; *phoc*, occipital phragma; *PT*, pretentorium; *PTH*, prothorax; *ptp*, posterior tentorial pit; *sdTA*, dorsal suspensor of anterior tentorium; *Slg*, superlingua (= anterior lobe of hypopharynx); *smTA*, middle suspensor of anterior tentorium; *spTA*, posterior suspensor of anterior tentorium; *st*, stipes; *TA*, anterior tentorium; *tm*; ventral suspensor; *TP*, posterior tentorium; *tpm*, tentorio-postmental muscle; *ts*, sagittal tendon of *advst1*; *ttm*, tentorio-mandibular muscle.

with $ds_{III/IV}$ is supported by its innervation from both the mandibular and maxillary ganglia (Bitsch, 1963).

The relative positions of the extrinsic appendicular muscles on the anterior tentorium are also consistent with these interpretations. The extrinsic antennal and pharyngeal dilator muscles attach to the anterior surface of the anterior tentorium (Fig. 7A,B,E: *antm, dvph*). The lateral tentorial surface receives mandibular muscles corresponding to ale_{III} and ame_{III} (Fig. 7A,E: *ttm3, ttm2*). The posterior surface of the anterior tentorium receives mandibular muscles corresponding to ple_{III} (Fig. 7A,E: *ttm1*) and maxillary muscles corresponding to ame_{IV} (Fig. 7A,D: *adca*). The second transverse connective ($tc_{III/IV}$) is retained and specialized as the transverse mandibular tendon (Fig. 7A,B,E: *ltm*), which links extrinsic mandibular muscles corresponding to pme_{III} (Fig. 7A,E: *adm*), and the transverse maxillary tendon (Fig. 7A,B,D: *ltmx*), which links extrinsic maxillary muscles corresponding to ame_{IV} (Fig. 7A,D: *adast*). The second ventral suspensor ($vs_{II/III}$) is retained as a pair of small ligaments (*tm*) that connects the transverse mandibular tendon (*ltm*) to the roof of the preoral chamber (Fig.7B,E).

The posterior tentorium (*TP*) is formed by ectodermal invaginations at the external attachment of $vs_{IV/V}$ and indicated externally by posterior tentorial pits (Fig. 7C: *ptp*) between the cranial articulations of the maxilla and labium (Larink, 1969). The invagination from each side is guided medially through the transverse connective ($ts_{IV/V}$), where they join to form a continuous transverse sclerite across the foramen magnum. The dorsal suspensor ($ds_{IV/V}$) corresponds to a muscle (Fig. 7A–C: *mld*) that arises from the dorsal margin of the posterior tentorium and attaches to the postgenal process (*pgp*) of the cranium. This scenario requires dorsal migration of $vs_{IV/V}$ and ventral elongation of $ts_{IV/V}$ to produce the observed adult structure (compare Fig. 7A,C: *TP*). It also requires that the anteroventral section of the transverse connective remain ligamentous to account for a mid-sagittal attachment (Fig. 7A,B,D: *ts*) for posterior adductors of the maxilla (Fig. 7A,D: *advst1*), which correspond to extrinsic muscle pme_{IV}. The ligament *ts* attaches to the transverse maxillary ligament (*ltmx*) by paired connectives corresponding to part of lc_{IV} (Fig. 7A,B).

As predicted by the model, the posterior surface of the posterior tentorium receives longitudinal connectives from the thorax (lc_V) in the form of paired ventral longitudinal muscles (Fig. 7A–C: *mth*) and two extrinsic labial muscles (Fig. 7A,C: *tpm*, *mprlb*) that correspond to ale_V and ame_V, respectively. Likewise, the anterior surface receives an extrinsic maxillary muscle (Fig. 7A,C,D: *advst2,3*) that corresponds to ple_{IV}. Muscles connecting the anterior face of the posterior tentorium with the posterior face of the anterior tentorium (Fig. 7A–C,E: *mtt*) may represent a portion of lc_{IV}.

Symphyla. The skeletomuscular anatomy of the symphylan head has been examined by Snodgrass (1951), Manton (1964) and Fanenbruck (2003). The study by Ravoux (1975) of *Scutigerella immaculata* is the most thorough and is used here in interpreting the cephalic endoskeleton. All muscles associated with the tentoria described by Ravoux are encompassed by this interpretation.

Interpretation (compare Figs. 1E, 8A, 9): The cephalic endoskeleton of symphylans appears to have undergone significant distortion associated with development from an original 'hypognathous' organization to the postembryonic sub-prognathous/entognathous condition (Tiegs, 1940). This change appears to entail a rotation of the original anterior-posterior axis to a anteroventral–posterodorsal axis and elongation of elements along the new axis. These transformations are depicted in Fig. 9. As described below, the relative positions of structures shown in Fig. 8A are retained despite this distortion.

The symphylan tentorium comprises two hollow, ventrally concave cuticular rods that span the length of the head (Fig. 8B: *TA*), each with a dorsal inflection near its posterior end. The rods develop anteriorly from ectodermal invaginations initiated at $vs_{II/III}$ near the hypopharynx (Fig. 8B,C: *hp*) and mandibles and are then guided through all cephalic longitudinal connectives (lc_I through lc_V) (Fig. 8A). The anterior end of each rod has a lateral process that engages the apodeme of the mandibular gnathal lobe (Fig. 8C), and a dorsal process equipped with three muscles (Fig. 8B: *sa1, sa2, sa3*) that attach to the cranial wall (Fig. 8B). Muscle *sa1* probably corresponds to $ds_{PO/I}$ (compare Figs. 8A, 9); it protracts the tentorium and abducts the gnathal lobes (Manton, 1964; Ravoux, 1975). Muscles *sa2* and *sa3* likely correspond to $ds_{I/II}$ (compare Figs. 8A, 9) and retract the tentorium. The posterior end of each rod receives a muscle (Fig. 8A–C: *116*) that arises from the dorsal cervical region and may correspond to $ds_{V/VI}$ of the groundplan. Manton (1964) claimed that this muscle attached to the dorsal cranial apodeme (Fig. 8B: *dap*), but Ravoux insisted that this is not the case.

The tentorial rods are joined transversely by two connective bridges, a large anterior bridge associated with the tentorial attachment of the extrinsic mandibular, maxilla 1 and maxilla 2 muscles and a small posterior bridge (Fig. 8: *atb*, *ptb*). Manton (1964) called the anterior bridge the 'transverse mandibular tendon' and the posterior bridge the 'transverse maxilla I tendon', but Ravoux (1975) found that all extrinsic endoskeletal muscles from all feeding appendages attach on the anterior bridge or adjacent regions of the tentorium and that no such muscles are associated with the posterior bridge. I propose that the two bridges are actually formed as part of a continuous structure that separated secondarily, a view supported by the common internal structure of the bridges. Specifically, each is comprised of three transverse sheets of connective tissue (dorsal, middle, ventral) (Figs. 8A, 9) that are distinct at their tentorial attachments and united medially.

The dorsal, middle and ventral connective layers of the tentorial bridges are interpreted here as transverse connectives $tc_{II/III}$, $tc_{III/IV}$ and $tc_{IV/V}$, respectively, that have elongated and assumed a roughly dorsal-to-ventral series rather than the original anterior-posterior series (Fig. 9). This transformation is reflected in the pattern of muscle attachment to the tentorial rods and bridges; those muscles that attach more dorsally on the exoskeleton attach more anteriorly on the exoskeleton (i.e., gnathal appendages or cranium). The dorsal layer ($tc_{II/III}$)

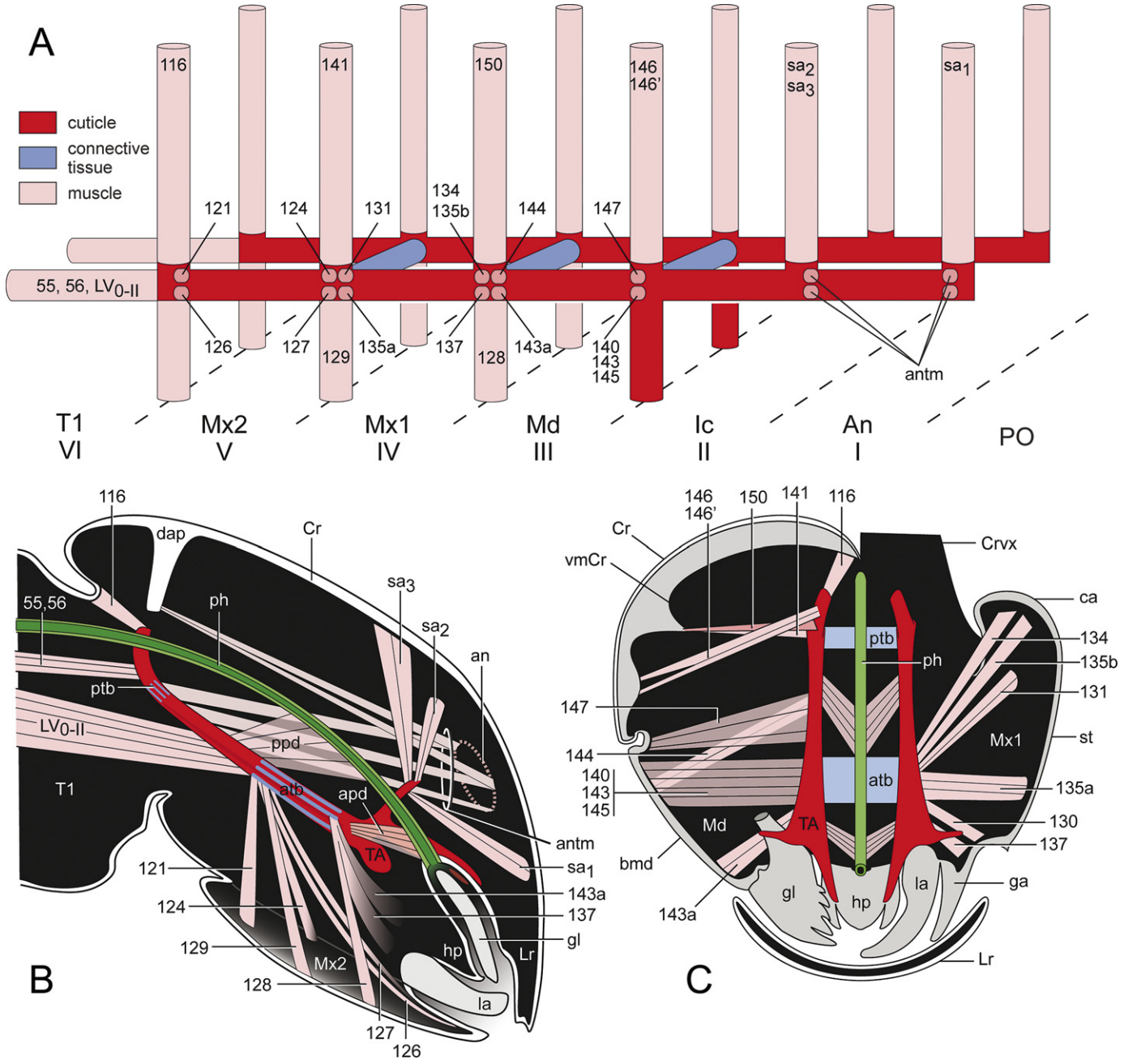

Fig. 8. Cephalic endoskeleton of Symphyla (Myriapoda). (A) Hypothetical mesodermal template of head endoskeleton showing proposed developmental fates of different components, where red is invaginated ectoderm (tentorium), blue is connective tissue and pink is muscle. Compare to Fig. 1E for proposed groundplan homologs. (B) Sagittal view of symphylan head (redrawn from Manton, 1964, modified according to Ravoux, 1975). (C) Dorsal view of frontal section of symphylan head (redrawn from Manton, 1964, modified according to Ravoux, 1975). Muscle names and numbering system follow Ravoux (1975). Abbreviations: *I–VI*, first to sixth postoral segments; *An*, antennal segment; *ant*, internal margin of antenna; *antm*, antennal muscles; *apd*, anterior pharyngeal dilator; *atb*, anterior tentorial bridge; *bmd*, basal part of mandible; *ca*, cardo; *Cr*, cranium; *Crvx*, cervix; *dap*, dorsal apodeme; *ga*, galea; *gl*, gnathal lobe of mandible; *hp*, hypopharynx; *la*, lacinia; *Lr*, labrum; *LV*, ventral longitudinal muscle; *Md*, mandible or mandibular segment; *Mx1*, maxilla 1 or maxilla 1 segment; *Mx2*, maxilla 2 ('labium') or maxilla 2 segment; *ph*, pharynx; *PO*, preoral structures; *ppd*, posterior pharyngeal dilator; *ptb*, posterior tentorial bridge; *sa*, anterior suspensor; *st*, stipes; *T1*, first trunk segment; *TA*, anterior tentorium; *vmCr*, ventral margin of cranium.

receives only the anterior/dorsal muscles of the mandible (ale_{III}, ame_{III}) (Fig. 8A,C: *147, 140 + 143 + 145*). The posterior/ventral mandibular muscles (ple_{III}, pme_{III}) (Fig. 8A,C: *144, 143a*) and anterior/dorsal maxilla 1 muscles (ale_{IV}, ame_{IV}) (Fig. 8A,C: *131, 135b*) attach on the tentorial rod laterally at the level of the middle connective ($tc_{III/IV}$), and the posterior/ventral maxilla 1 muscles (ple_{IV}, pme_{IV}) (Fig. 8A,C: *134, 130 + 137*) and all maxilla 2 muscles (ale_{V}, ame_{V}, ple_{V}, pme_{V}) (Fig. 8A,B: *124, 127, 121, 126*) attach to the ventral surface of the tentorial rods and the ventral connective layer ($tc_{IV/V}$). This is particularly striking in cross sections illustrated by Ravoux (1975: figs 7 and 13). Identifying

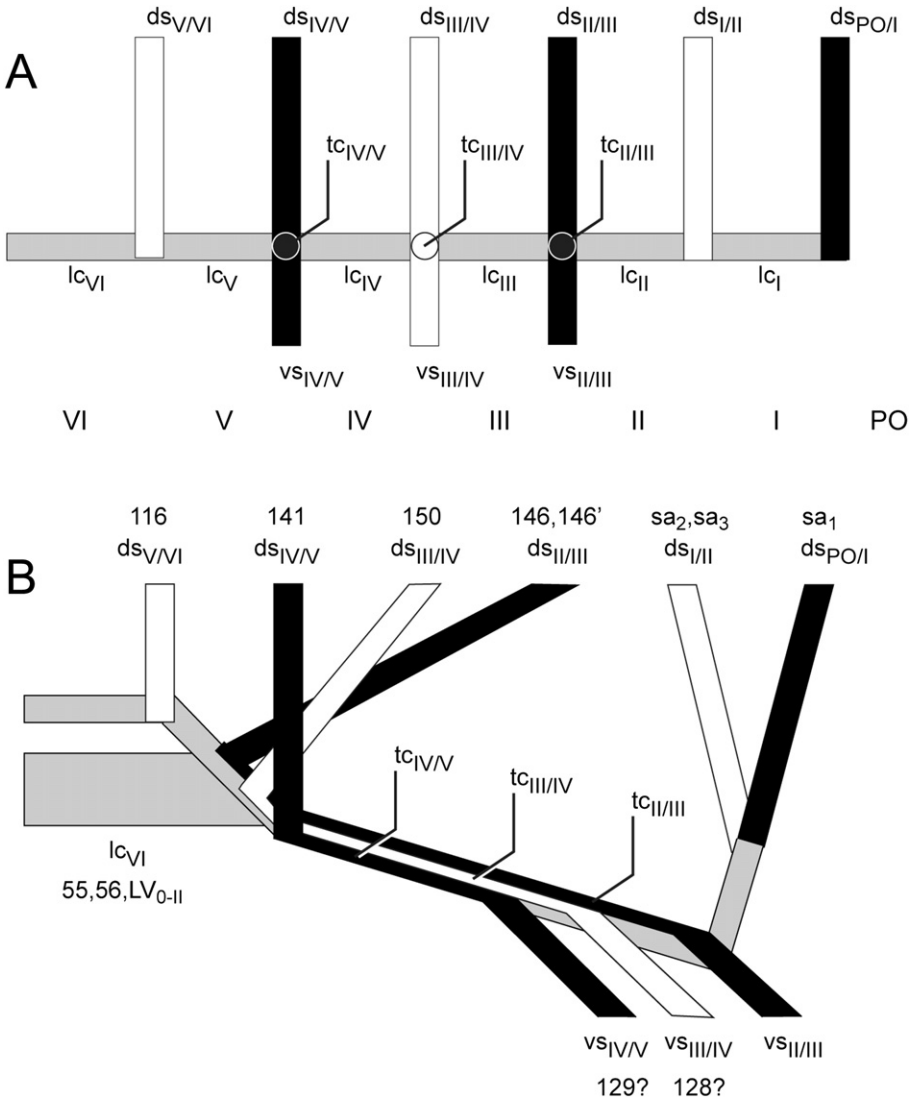

Fig. 9. Distortion of the symphylan cephalic endoskeleton. (A) Proposed undistorted groundplan for the symphylan head (compare with Figs. 1E, 8A) from medial perspective. (B) Proposed distortion associated with transition from hypognathous to prognathous mouthparts and elongation of skeletal axis. Abbreviations: *I–VI*, first to sixth postoral segments; *ds*, dorsal suspensor; *lc*, longitudinal connective; *tc*, transverse connective; *vs*, ventral suspensor. Muscle abbreviations or numbers follow Ravoux (1975). See Fig. 8.

possible homologs to $vs_{III/IV}$ and $vs_{IV/V}$ is problematic, but these likely occur among the 'extra' extrinsic muscles of maxilla 2. Specifically, *128* shares a ligamentous attachment to the anterior tentorial bridge (*atb*) with maxilla I muscle *137* ($= ame_{IV}$) and mandibular muscle *143a* ($= pme_{III}$) (Fig. 8A,B) (Ravoux, 1975: his fig 18) suggesting that *128* corresponds to $vs_{III/IV}$ (see Fig. 8A). Muscle *129* has a near-median attachment on maxilla 2, posterior to the similarly positioned *128* (Fig. 8B), and an extreme posterior attachment to the anterior tentorial bridge, which it shares with the remaining maxilla 2 muscles (Fig. 8B), it is the most likely candidate for $vs_{IV/V}$.

The posterior tentorial bridge (Fig. 8B,C: *ptb*) has effectively the same internal structure as the anterior bridge (i.e., three dorsoventrally arranged sheets separate at their lateral tentorial attachments but united medially). However, the posterior bridge and adjacent tentorial rods are associated with dorsal suspensor muscles that attach sequentially along the subvertical portion of each rod; those with a more dorsal tentorial attachment have a more anterior attachment to ventrolateral margin of the cranial sclerite (Fig. 8C). These muscles (i.e., *146 + 146′, 150, 141*) likely correspond to $ds_{II/III}$, $ds_{III/IV}$ and $ds_{IV/V}$, respectively. This is consistent with the proposal that the anterior and posterior bridges are remnants of an originally continuous three-layered structure. Specifically, the dorsal connective layer of each bridge receives muscles expected to be associated with the first transverse connective ($tc_{II/III}$), namely, the anterior extrinsic muscles of the mandible and a dorsal suspensor with an anterior exoskeletal attachment. Muscles associated with the middle and ventral layers show the same consistent pattern (compare Figs. 8A, 9).

The location and fate of ventral suspensors $vs_{III/IV}$ and $vs_{IV/V}$ is problematic, but if they persist in the adult, they are likely to be found among the extrinsic muscles of maxilla 2. Muscle *128* (Fig. 8A,B) is a particularly compelling candidate for $vs_{III/IV}$ as

it has a distinct anterior median attachment to maxilla 2 and shares a tendinous attachment to the anterior tentorial bridge with a posterior mandibular muscle (*143a*) and an anterior maxilla 1 muscles (*137*). The extreme anterior attachment of *128* is unique among extrinsic muscles of maxilla 2. Muscle *129* is similar to *128* in having a near-median ventral attachment but differs from *128* attaching more posteriorly to both maxilla 2 and the anterior tentorial bridge. Thus it is a reasonable candidate for $vs_{IV/V}$.

Acknowledgments

This work was supported by the Maryland Agricultural Experiment Station, the General Research Board of the University of Maryland, and National Science Foundation Grant 0416628 to Susan Masta (Portland State University).

References

Abd el-Wahab, A., 1952. Notes on the morphology of the scorpion, *Buthus quinquestriatus* (H.E.). Publications de l'Institut Fouad 1er du Desert 3, 1–129.

Adams, J.C., Watt, F.M., 1993. Regulation of development and differentiation by the extracellular matrix. Development 117, 1183–1198.

Anderson, J.F., Prestwich, K.N., 1975. The fluid pressure pumps of spiders (Chelicerata, Araneae). Zeitschrift für Morphologie der Tiere 81, 257–277.

Barrows, W.M., 1925. Modification and development of the arachnid palpal claw, with especial reference to spiders. Annals of the Entomological Society of America 18, 483–516.

Bitsch, C., Bitsch, J., 2002. The endoskeletal structures in arthropods: cytology, morphology and evolution. Arthropod Structure and Development 30, 159–177.

Bitsch, J., 1963. Morphologie céphalique des Machilides (Insecta Thysanura). Annales des Sciences Naturelles, Zoologie. 12 ser 5, 501–706.

Börner, C., 1904. Beiträge zur Morphologie der Arthropoden. I. Ein Beitrag zur Kenntnis der Pedipalpen. Zoologica 42, 1–174.

Boudreaux, H.B., 1979. Significance of intersegmental tendon system in arthropod phylogeny and a monophyletic classification of Arthropoda. In: Gupta, A.P. (Ed.), Arthropod Phylogeny. Van Nostrand Reinhold, New York, pp. 551–586.

Brauer, A., 1895. Beiträge zur Kenntnis der Entwicklungsgeschichte des Skorpiones, II. Zeitschrift für wissenschaftliche Zoologie 59, 351–433.

Chaudonneret, J., 1950. La morphologic céphalique de Thermobia domestica (Packard) (Insecte, Aptérygote, Thysanoure). Annales Sciences Naturelles, Zoologic et Biologic Animale Sér. 1112, 145–302.

Cisne, J.L., 1974. Trilobites and the origin of arthropods. Science 186, 13–18.

Cisne, J.L., 1981. *Triarthrus eatoni* (Trilobita): anatomy of its exoskeletal, skeletomuscular, and digestive systems. Palaeontographica Americana 9 (53), 1–142.

Cole, A.J., Hall, B.K., 2004a. Cartilage is a metazoan tissue; integrating data from nonvertebrate sources. Acta Zoologica 85, 69–80.

Cole, A.J., Hall, B.K., 2004b. The nature and significance of invertebrate cartilages revisited: distribution and histology of cartilage and cartilage-like tissues within the Metazoa. Zoology 107, 261–273.

Couzijn, H.W.C., 1976. Functional anatomy of the walking-legs of Scorpionida with remarks on terminology and homologization of leg segments. Netherlands Journal of Zoology 26, 453–501.

Dubale, M.S., Vyas, A.B., 1968. The structure of the chela of *Heterometrus* sp. and its mode of operation. Bulletin Southern California Academy of Sciences 67, 240–244.

Fanenbruck, M., 2003. Die Anatomie des Kopfes und des cephalen Skelett-Muskelsystems der Crustacea, Myriapoda und Hexapoda: Ein Beitrag zum phylogenetischen System der Mandibulata und zur Kenntnis der Herkunft der Remipedia und Tracheata. Unpublished doctoral dissertation, Ruhr-Universitaet Bochum, 450 pp.

Farley, R.D., 1999. Scorpiones. In: Harrison, F.W., Foelix, R.F. (Eds.), Microscopic Anatomy of Invertebrates. Chelicerate Arthropods, vol. 8A. Wiley-Liss, New York, pp. 117–222.

Firstman, B., 1954. The central nervous system, musculature and segmentation of the cephalothorax of a tarantula (*Eurypelma californicum* Ausserer). Microentomology 19, 1–40.

Firstman, B., 1973. The relationship of the chelicerate arterial system to the evolution of the endosternite. Journal of Arachnology 1, 1–54.

Garcia-Alonso, L., Fetter, R.D., Goodman, C.S., 1996. Genetic analysis of Laminin A in *Drosophila*: extracellular matrix containing laminin A is required for ocellar axon pathfinding. Development 122, 2611–2621.

Hessler, R.R., 1964. The Cephalocarida: comparative skeletomusculature. Memoirs of the Connecticut Academy of Arts and Science 16, 1–97.

Hjelle, J.T., 1990. Anatomy and morphology. In: Polis, G.A. (Ed.), The Biology of Scorpions. Stanford Univ. Press, Stanford, CA, pp. 9–63.

Kästner, A., 1931. Die Hüfte und ihre Umformung zu Mundwerkzeugen bei den Arachniden. Versuch einer Organgeschichte. Zeitschrift für Morphologie und Ökologie der Tiere 22, 721–758.

Koch, M., 2000. The cuticular cephalic endoskeleton of primarily wingless hexapods: ancestral state and evolutionary changes. Pedobiologia 44, 374–385.

Kresse, H., Schönherr, E., 2001. Proteoglycans of the extracellular matrix and growth control. Journal of Cellular Physiology 189, 266–274.

Lankester, E.R., Benham, W.B.S., Beck, E.J., 1885. On the muscular and endoskeletal systems of *Limulus* and *Scorpio*; with some notes on the anatomy and generic characters of scorpions. Transactions of the Zoological Society of London Part 10 11, 311–390.

Larink, O., 1969. Zur Entwicklungsgeschichte von *Petrobius brevistylis* (Thysanura, Insecta). Helgoländer wissenschaftliche Meeresuntersuchungen 19, 111–155.

Leptin, M., Bogaert, T., Lehmann, R., Wilcox, M., 1989. The function of PS integrins during *Drosophila* embryogenesis. Cell 56, 401–408.

Manton, S.M., 1964. Mandibular mechanisms and the evolution of arthropods. Philosophical Transactions of the Royal Society of London, Series B 247, 1–183.

Millot, J., 1942a. Sur l'anatomie et l'histophysiologie de *Koenenia mirabilis* Grassi (Arachnida Palpigradi). Revue Francaise d'Entomologie 9, 33–51.

Millot, J., 1942b. Notes complémentaires sur l'anatomie, l'histologie et la répartition géographique en France de *Koenenia mirabilis* Grassi. Revue Francaise d'Entomologie 9, 127–135.

Palmgren, P., 1978. On the muscular anatomy of spiders. Acta Zoologica Fennica 155, 1–41.

Parry, D.A., Brown, R.H.J., 1959. The hydraulic mechanism of the spider leg. Journal of Experimental Biology 36, 423–433.

Petrunkevitch, A., 1922. The circulatory system and segmentation in Arachnida. Journal of Morphology 36, 157–186.

Pocock, R.I., 1902. Studies on the arachnid endosternite. Quarterly Journal of Microscopical Science 46, 225–262.

Prestwich, K.N., 1988. The constraints on maximal activity in spiders. I. Evidence against the fluid insufficiency hypothesis. Journal of Comparative Physiology B 158, 437–447.

Ravoux, P., 1975. Endosquelette et musculature céphaliques de *Scutigerella immaculata* Newport (Symphyla: Scutigerellidae). Bulletin du Muséum National d'Histoire Naturelle, 3 ser., No. 332. Zoologie 234, 1189–1238.

Riley, W.A., 1904. The embryological development of the skeleton of the head of *Blatta*. American Naturalist 38, 777–810.

Sensenig, A., Shultz, J.W., 2003. Mechanics of cuticular elastic energy storage in leg joints lacking extensor muscles in arachnids. Journal of Experimental Biology 206, 771–784.

Sensenig, A., Shultz, J.W., 2004. Mechanics of elastic extension in the pedipalpal joints of scorpions and solifuges (Arachnida: Scorpiones, Solifugae). Journal of Arachnology 32, 1–10.

Sheetz, M.P., Felsenfeld, D.P., Galbraith, C.G., 1998. Cell migration: regulation of force on extracelluar-matrix-integrin complexes. Trends in Cell Biology 8, 51–56.

Shultz, J.W., 1989. Morphology of locomotor appendages in Arachnida: evolutionary trends and phylogenetic implications. Zoological Journal of the Linnean Society 97, 1–56.

Shultz, J.W., 1991. Evolution of locomotion in Arachnida: the hydraulic pressure pump of the giant whipscorpion, *Mastigoproctus giganteus* (Uropygi). Journal of Morphology 210, 13–31.

Shultz, J.W., 1993. Muscular anatomy of the giant whipscorpion, *Mastigoproctus giganteus* (Arachnida, Uropygi), and its evolutionary significance. Zoological Journal of the Linnean Society 108, 335–365.

Shultz, J.W., 1999. Muscular anatomy of a whipspider, *Phrynus longipes* (Pocock) (Arachnida: Amblypygi), and its evolutionary significance. Zoological Journal of the Linnean Society 126, 81–116.

Shultz, J.W., 2000. Skeletomuscular anatomy of the harvestman *Leiobunum aldrichi* (Weed, 1893) (Arachnida: Opiliones) and its evolutionary significance. Zoological Journal of the Linnean Society 128, 401–438.

Shultz, J.W., 2001. Gross muscular anatomy of *Limulus polyphemus* (Xiphosura, Chelicerata) and its bearing on evolution in the Arachnida. Journal of Arachnology 29, 283–303.

Shultz, J.W., Pinto da Rocha, R. Morphology and functional anatomy, In: Pinto da Rocha, R., Machado, G., Giribet, G. (Eds), The Harvestmen: The Biology of Opiliones, Harvard University Press, Cambridge, MA, in press.

Snodgrass, R.E., 1928. Morphology and evolution of the insect head and its appendages. Smithsonian Miscellaneous Collections 81 (3), 1–158.

Snodgrass, R.E., 1948. The feeding organs of Arachnida, including mites and ticks. Smithsonian Miscellaneous Collections 110 (10), 1–93.

Snodgrass, R.E., 1950. Comparative studies of jaws of mandibulate arthropods. Smithsonian Miscellaneous Collections 116 (1), 1–85.

Snodgrass, R.E., 1951. Comparative studies on the head of mandibulate arthropods. Comstock Publishing Co., Inc., Ithaca, NY.

Snodgrass, R.E., 1958. The evolution of arthropod mechanisms. Smithsonian Miscellaneous Collections 138 (2), 1–77.

Snodgrass, R.E., 1960. Facts and theories concerning the insect head. Smithsonian Miscellaneous Collections 142 (1), 1–61.

Stewart, D.M., Martin, A.W., 1974. Blood pressure in the tarantula, *Dugesiella hentzi*. Journal of Comparative Physiology 88, 141–172.

Stockwell, S.A., 1989. Revision of the phylogeny and higher classification of scorpions (Chelicerata). Unpublished doctoral dissertation, University of California at Berkeley, 413 pp.

Tiegs, O.W., 1940. The embryology and affinities of the Symphyla, based on a study of *Hanseniella agilis*. Quarterly Journal of Microscopical Science 82, 1–225.

Umemiya, T., Takeichi, M., Nose, A., 1997. M-Spondin, a novel ECM protein highly homologous to vertebrate F-Spondin, is localized at the muscle attachment site in the *Drosophila* embryo. Developmental Biology 186, 165–176.

Vorbrüggen, G., Jäckle, H., 1997. Epidermal muscle attachment site-specific target expression and interference with myotube guidance in response to ectopic *stripe* expression in the developing *Drosophila* epidermis. Proceedings of the National Academy of Science USA 94, 8606–8611.

Vyas, A.B., 1970. Studies in Myology of the Scorpion *Heterometrus fulvipes* Koch. Unpublished doctoral dissertation, Gujarat University, India, 256 pp.

Vyas, A.B., 1974. The cheliceral muscles of the scorpion *Heterometrus fulvipes*. Bulletin. Southern California Academy of Sciences 73, 9–14.

Weygoldt, P., Paulus, H.F., 1979. Untersuchungen zur Morphologie, Taxonomie und Phylogenie der Chelicerata. Zeitschrift für Zoologische Systematik und Evolutionsforschung 17, 85–116, 177–200.